The MESSENGER Magnetic Fields Experiment

B. J. Anderson[1], D. A. Lohr[1], M. H. Acuna[2], J. Scheifele[2], A. Raval[1], and H. Korth[1]

1. The Johns Hopkins University Applied Physics Laboratory, 11100 Johns Hopkins Road, Laurel Maryland, 20723

2. Goddard Space Flight Center, Greenbelt Maryland

To be submitted to Planetary and Space Science

Draft of 1 March 2005

Abstract: The Magnetometer (MAG) instrument on the MErcury Surface Space ENvironment and Ranging (MESSENGER) mission is a low noise tri-axial fluxgate magnetometer tailored to the mission's science objectives and operational constraints. The primary MESSENGER science objective addressed by MAG is the characterization of the structure of Mercury's intrinsic magnetic field. The Mariner 10 observations indicate a planetary moment in the range 170 to 350 nT-R_m^3 where R_m is a Mercury mean radius. The presence of an intrinsic field was a major finding since the expectation had been that the core was completely solid. The factor of two uncertainty in the dipole moment makes it difficult to reliably infer higher order terms that are of great interest for understanding the history and dynamics of the planet. By orbiting Mercury, MESSENGER will provide detection of higher order moments contributing as little as 1% to the surface magnetic field [*Korth et al.*, 2004]. To achieve this objective MAG uses a very low noise sensor yielding accuracy better than 3 nT and orientation knowledge accurate to better than 0.5° with 0.1° accuracy anticipated from in-flight characterization. To facilitate pre-launch testing MAG has two ranges: a coarse range for ground testing, ±51,300 nT full scale, 1.6 nT resolution; and a fine range for operation at Mercury, ±1,530 nT, 0.047 nT resolution. The MAG sensor is mounted at the end of a 3.6 meter long two-hinge boom to minimize spacecraft contamination fields. For operational reasons boom deployment is scheduled to occur in March 2005. Compensation magnets were used to ensure that the residual spacecraft field at the sensor will be less than a few nT. The fixed residual field will be characterized in flight and is easily corrected in ground processing. Spacecraft variable fields were mitigated with a magnetics cleanliness program involving the power system, attitude system, payload and harness to achieve dynamic contamination below the MAG fine range resolution. To accommodate variable telemetry volume allocations, MAG provides eleven sampling output rates from 0.01/s to 20/s. Data output more coarsely than one sample per second are sub-samples of 0.5 Hz low pass digitally filtered data. Sampling from 1/s to 10/s employs digital anti-alias filtering appropriate to the Nyquist frequency of the output rate. The analog signals from the three axes are separately analog low pass filtered at 10 Hz and sampled simultaneously by three independent 20-bit A/D converters every 50 ms. Strict even time sampling is ensured by a clock internal to MAG. Data are time tagging to within ±25ms of the spacecraft clock. To provide continuous information on fluctuations up to 10 Hz MAG provides a 1-10 Hz pass band average amplitude channel for one axis selected by command. This AC amplitude is also used to allow triggered sampling of 20/s data in eight minute windows allowing waveform capture of events during portions of the orbit or mission when continuous high rate sampling is not possible. The MAG instrument will therefore provide accurate characterization of the intrinsic field, magnetospheric structure and dynamic processes throughout Mercury's magnetosphere and its boundaries with the solar wind plasma.

1. Introduction

The discovery of Mercury's intrinsic magnetic field in 1974 by Mariner 10 [*Ness et al.*, 1974] was something of a surprise since the planet's size seemed to rule out the possibility of an active dynamo [*Solomon*, 1976; *Srnka*, 1976; *Jackson and Beard*, 1977]. Subsequent measurements from the 1975 Mariner 10 flyby [*Ness et al.*, 1975, 1976] strongly confirmed the initial conclusions and allowed evaluation of the planetary moment to within perhaps a factor of two [*Connerney et al.*, 1988]. The discovery prompted various suggestions to account for the intrinsic field. Remanent magnetization of the crust and mantle was proposed [*Stephenson*, 1976]. To account for a permanent dipole moment of the intensity observed, the remanent magnetization would either have to deviate from proportionality to the now extinct internal magnetizing field or would need to have a non-uniform thickness of magnetized material [*Runcorn*, 1975a, 1975b; *Stephenson et al.*, 1983; *Stephenson*, 1983; *Aharonson et al.*, 2004]. It may also be that the presence of Sulfur in the outer core would allow a thin outer fluid core to persist to the present time which could support a shell dynamo [*Stephenson*, 1987]. In an effort to constrain these hypotheses more sophisticated analysis of the Mariner 10 data were performed [*Wang*, 1977; *Engle*, 1997] but as *Connerney et al.* [1988] pointed out it is not possible to derive more precise estimates of the dipole and higher order moments from the Mariner because the two trajectories do not adequately constrain the inversion [*Connerney et al.*, 1988; *Korth et al.*, 2004].

The only way to better constrain the intensity and structure of Mercury's intrinsic magnetic field is to measure the magnetic field from an orbiting platform. Conducting these measurements is one of the primary science objectives of the MESSENGER mission [*Solomon et al.*, 2001; *Gold et al.*, 2001]. This paper describes the magnetic field investigation (MAG) included in the MESSENGER payload covering the performance requirements, instrument design including mechanical, sensor boom, electronics, software, spacecraft magnetic cleanliness program, pre-launch testing and initial performance in space. Post-launch instrument calibration activities are ongoing and will include observations during the Earth encounter scheduled for 2 August 2005. A comprehensive discussion of instrument calibration will be presented following this event.

2. Science Objectives, Instrument Requirements, Mission Constraints

2.1 Mercury Intrinsic Magnetic Field

The primary science objective of MAG is to measure the structure of Mercury's magnetic field to constraining higher order moments and identify crustal remanent fields. The Mariner 10 flyby observations indicate that the planetary moment is in the range 170 to 350 nT-R_m^3 where (R_m is the planet's radius) and is aligned with the planetary rotation axis to within about 11^o [*Ness et al.*, 1975, 1976; *Connerney*, 1988; *Korth et al.*, 2004]. The large range of dipole values reflects different assumptions regarding higher order terms which cannot be uniquely resolved with the Mariner 10 trajectories [*Connerney*, 1988]. Over the planet's pole the magnetic field magnitude is expected to be ~600 nT and ~300 nT at the equator. The orbital coverage provided by the MESSENGER mission will allow determination of the planetary dipole moment to 10-20% without any correction for the external field [*Korth et al.*, 2004]. This improvement over the uncertainties in determinations from the Mariner 10 data is required to evaluate higher order structure in the field. At this level higher order structure in the field smaller than ~20% of the dipole strength could not be distinguished from external field contributions.

The accuracy and orientation precision required for MAG are determined by the intensity of Mercury's magnetic field and the variable contributions due to external currents. The magnetospheric currents are expected to respond promptly to the imposed solar wind and interplanetary magnetic field (IMF) [*Luhmann et al.*, 1998; *Glassmeier*, 2000]. The external currents contribute fields as large as ~2/3 of the intrinsic field at the surface near the equator on the nightside [e.g. *Ness et al.*, 1974]. By contrast, at Earth the external currents generate fields that are typically less than 1% of the intrinsic field at the surface. Relative to the planetary radius Mercury's magnetosphere is about 15% as large in linear dimension as Earth's [e.g. *Slavin et al.*, 1979]. The external currents contribute a large, variable background signal and are the primary limiting factor in determining the structure of Mercury's intrinsic magnetic field for the MESSENGER orbit [*Korth et al.*, 2004].

2.2 Magnetospheric Magnetic Fields

2.2.1 Fields Due to External Currents

Determination of higher order moments requires specification of and correction for the external magnetic field. Characterizing the structure of the magnetospheric field is therefore a necessary component of the science objective because it enables extraction of higher order moments of the intrinsic planetary magnetic field. The statistical uncertainty in the inverted moment, including the effective noise contribution due to variable solar wind and interplanetary magnetic field (IMF) conditions at Mercury, allows unambiguous identification of quadrupole and octupole moments from the MESSENGER orbit yielding contributions larger than ~1% of the dipole intensity at the surface [*Korth et al.*, 2004]. It is therefore necessary to measure Mercury's magnetic field to an accuracy of ~1% of the planetary moment, that is, 3 to 6 nT for the expected planetary moment.

2.2.2 Magnetospheric Boundaries, Currents Waves

There are several secondary science objectives which the magnetic field measurements address [*Russell et al.*, 1988]. These include: wave particle interactions both associated with field line resonances which should have periods comparable to ion gyro-periods (~1 to 7 Hz for protons) [*Glassmeier et al.*, 2003] and those associated with heavy ions in Mercury's exosphere that may play a role in the formation of the exosphere [*Potter and Morgan*, 1990]; magnetotail dynamics possibly analogous to substorms in Earth's magnetosphere [*Ogilvie et al.*, 1975; *Christon*, 1987]; magnetopause structure and dynamics for Mercury's small magnetosphere (compared both to the planet and to energetic ion gyroradii) under the solar wind conditions that generally prevail at Mercury [*Siscoe and Christopher*, 1975; *Slavin et al.*, 1979; *Burlaga*, 2001] and which are very different from the average conditions prevailing at Earth and the outer planets; and characterization of field aligned currents linking the planet with the magnetosphere which are of great interest since they can provide insight into the interaction of a planet having no ionosphere with the magnetosphere/solar wind dynamo [*Slavin et al.*, 1997]. Wave amplitudes are expected to be near 1 nT, occasionally larger. Magnetopause turbulence is expected to be several nT in amplitude and extends up to and above ion gyrofrequencies (~2 Hz). Magnetotail dynamics has signatures of a few to 10s of nT and occur on time scales of seconds to minutes. Field aligned currents may have signatures as small as a few nT or as large as 10s of nT and the regions of interest will be traversed in a few minutes. The MAG instrument should therefore provide for measurements above a few Hz and have sufficient resolution to resolve ~1 nT amplitude waves.

2.3 Observational Requirements

The MAG characteristics were tailored to the scientific objectives but the instrument was also designed to be easy to test and to make efficient use of limited spacecraft telemetry [*Santo et al.*, 2001; *Gold et al.*, 2001]. The dynamic range and resolution of the instrument are determined by the expected detectable structure of Mercury's magnetic field. To support measurements over the range of expected fields at Mercury and conduct measurements during test and integration, MAG is equipped with two ranges: coarse, covering ±51,300 nT, and fine, covering ±1,530 nT. An accuracy of 3 nT corresponds to 0.2% in the sensitive range. The accuracy objective imposes a requirement that the spacecraft magnetic field at the MAG sensor vary by less than ~1 nT and that the sensor orientation knowledge requirement be commensurate with 1% error (~600 nT maximum field) corresponding to 0.6°. Detection of waves with amplitudes of 1 nT requires resolution below 1 nT, of the order of 0.1 nT at least. The MAG instrument provides 1.6 nT resolution in coarse range and 0.047 nT resolution in fine range and the gain factors were determined to an accuracy of 0.01% and 0.08% in coarse and fine range, respectively.

2.4 Mission Operations Constraints

To meet the science objectives within mission telemetry constraints MAG provides a range of sampling rates. At the minimum altitude of 200 km, the MESSENGER speed relative to the surface will be ~3 km/s, implying that a resolution comparable to roughly half the altitude is provided by a 30s sampling interval. However, characteristic time scales of Mercury's magnetosphere and signatures at the magnetospheric boundary are much shorter, a few seconds to fractions of a second, and wave particle interactions (the proton gyrofrequency at 500 nT is about 7.5 Hz) so sampling with a Nyquist frequency higher than a few Hz is strongly desired. The magnetic field data is also required to interpret data acquired by the MESSENGER Energetic Particle Spectrometer (EPS) which has a minimum sample interval of 0.5s for the electron channels. It is therefore strongly desired to have sampling of 1/s with options to sample faster than 10/s. During the mission cruise phase however, calibration of the spacecraft magnetic field requires long term observations of the interplanetary magnetic field which can be accommodated using very low time resolution observations. MAG therefore uses selectable filter and sub-sampling techniques providing output sample rates from 0.01/s to 20/s.

To ensure that spacecraft fields at the MAG sensor are sufficiently stable to meet the science objectives, the MAG sensor is mounted on a boom that extends 3.6 meters from the spacecraft as shown in Figure 1 which also shows the spacecraft (SC) coordinate system. The boom extends in the +Y direction which is nominally anti-sunward during the mission's orbital phase. The payload adapter ring which also houses remote sensing instruments is on the +Z end of the spacecraft. The +X direction completes the right hand system. The MAG axes were chosen to correspond to the spacecraft system with only small corrections required to account for slight mounting uncertainties.

During orbital operations the spacecraft can be turned slightly so that +Y is not strictly anti-sunward. To protect the MAG sensor from direct exposure to solar illumination at Mercury, a small shade is mounted near the sensor. The shade frame is made of non-magnetic single alloy Titanium and the shade itself is a non-conducting ceramic fabric so this structure will not generate thermo-electric currents. Steps were also taken to ensure that the sensor and cabling could survive an unexpected attitude anomaly at Mercury that might place the boom and sensor in direct sunlight. All cabling was tested to ensure structural and electrical integrity were preserved on direct exposure to solar illumination at Mercury. Thermal balance tests of the blanketed sensor show that its temperature would remain below

150^{o}C, below the temperature rating of all sensor components. During normal operations the sensor will be cooled passively and is expected to be regulated by the sensor heater to stay at –15^{o}C. Instrument gain and offset stability for the sensor (determined principally by the core materials and characterized for previous missions, e.g. Voyager) are excellent yielding less than 0.25% change in gain over the entire range –40^{o}C to +50^{o}C and a change in offset of less than 2 nT in 50C^{o}. Use of room temperature calibrations therefore meets the science requirements for MESSENGER.

3. Hardware Description

The MESSENGER Magnetometer (MAG) is a three axis fluxgate magnetometer based on heritage from the Advanced Composition Explorer (ACE), Wind and Near Earth Asteroid Rendezvous Shoemaker (NEAR-Shoemaker) spacecraft. For MESSENGER, MAG employs somewhat miniaturized electronics to minimize mass resources. Essential instrument characteristics are summarized in Table 1. The instrument consists of an electronics box and sensor is mounted at the end of the boom. Figure 2 shows a block diagram of the instrument electronics. The electronics includes the fluxgate analog drive/sense circuitry for two gain states, fine and coarse, analog to digital conversion and associated programmable gate arrays, oscillator clock and dividers, experiment processing unit (EPU) including on-board memory, power converter, sensor survival heater drive with thermostatic control, and interface to the payload data processing unit (DPU).

3.1 Sensor and Boom

The sensor is shown in the left panel of Figure 3 and uses three ring cores centered in corresponding nulling and sense coils. The three sensors' axes are orthogonal (fixed) to better than 0.2^{o} (0.01^{o}) and signals from the three sensors are converted to a strictly orthogonal system based on ground calibration. A multi-layer heater element is integrated with the sensor to maintain the sensor above its minimum operating temperature of –40^{o}C. The heater set point is –15^{o}C. When shaded the sensor is expected to cool passively below –15^{o}C so the heater will normally be operating to hold the sensor near –15^{o}C. The sensor survives exposure to lower temperatures down to –100^{o}C without degradation in alignment or calibration. The sensor frame material ensures close temperature coefficient matching to the windings of the nulling and sense coils and survival at temperatures up to 150^{o}C. Tests exposing a blanketed mass matched in size and heat capacity to the sensor to 11 Sun illumination, equivalent to the maximum insolation at Mercury, were performed showing a six hour rise time from –15^{o}C to 120^{o}C. The sensor was operated without adverse affects from –100^{o}C to +50^{o}C in environmental testing. To prevent continuous exposure to direct sunlight, a sensor shade is included, mounted to the boom just below the sensor as shown in Figure 4.

The boom is carbon composite tubing in two sections with two spring loaded hinges. The inboard hinge is mounted at the spacecraft and the outboard hinge is near the mid-point of the boom. The outboard hinge with the cable service loop is shown in Figure 4 in the deployed configuration prior to installation of thermal blankets. Each hinge is composed of non-magnetic materials, including spring, locking pin, frame and damper. The spring is pre-loaded to provide restoring torque to angular displacement from the deployed position in either direction. The neutral, deployed position is established with flats and a twist damper dissipates energy released on deployment. Deployment repeatability was <0.05^{o} in pre-launch tests. Locking pins secure both hinges after deployment to avoid any hinge bending during propulsive maneuvers after deployment.

Cabling between the sensor and electronics is threaded inside the boom and service loops at both hinges allow free hinge motion (cf. Figure 4). The boom is thermally blanketed and the cabling at the middle hinge service loop is also blanketed. The coaxial fluxgate drive and sense cables and other wiring for temperature sensing and heater power were all tested on exposure to 11 Sun illumination and rose to 155^{o}C after six hours of exposure to 11 Suns and were exposed to a maximum of 180^{o}C. The cabling suffers no deterioration from exposure to intense solar illumination or temperatures up to 280^{o}C. The drive cable contributes 1.5% of the resonant drive circuit capacitance. The change in cable capacitance over the full temperature range changes the resonant frequency by less than 0.01%. The Q of the resonance was chosen to ensure proper operation over the full range of cable and sensor temperatures.

3.2 Electronics

The electronics is housed in a chassis composed of slices with 4" x 4" electronics boards integrated with the chassis frame and connectors. The complete electronics box is the stack of slices for the power converter, sensor survival heater circuit, EPU and interface to the payload DPU, A/D converter and digital control logic and anlog electronics. The Low Voltage Power Supply (LVPS) provides power to the EPU and MAG electronics under spacecraft control. The MAG EPU interfaces with the LVPS via an inter-integrated computer (I2C) bus to collect MAG probe temperature, electronics temperature, MAG DC/DC current and 3-axis magnetic field samples with 14 bit resolution. Figure 3 shows the electronics with the end cover removed to show the analog electronics slice. Miniature coupling transformers were used to achieve this degree of miniaturization and are visible in this view. The complete electronics package volume is less than 1200 cm^3 and its mass is under 850 g.

3.2.1 Analog Electronics

Figure 5 shows a functional schematic of the MAG electronics with detail of the analog synchronous detection electronics. The three ring core excitation coils are driven by the same 15 kHz drive which is obtained from a divide by two from 30 kHz. The 30 kHz signal is input to the synchronous detection electronics to capture the 30 kHz response of each of the sense coils for the three axes. Each axis has its own detection electronics which generates a negative feedback voltage that is used to drive a current through the corresponding solenoid nulling coil. The voltage driving this current is proportional to the magnetic field. The intrinsic noise of the fluxgate sensor is ~10 pT. To accommodate the possible temperature extremes experienced at Mercury, the fluxgate tuning was relaxed somewhat to be less sensitive to temperature variations at the expense of some sensitivity so the sensitivity of the analog system is ~20 pT.

There are two sets of amplifiers, one with a full scale of ~ ±66,000 nT for use in ground testing and the other with a full scale of ~ ±2,000 nT suitable for measuring Mercury's magnetic field. These ranges are digitized to ±51,300 and ±1,530 nT with the resolutions shown in Table 1. The range is selected by a discrete signal to the analog electronics and is the same for all three axes. The timing latency of the detection and feedback system is 3.2 ms. The instrument includes an analog calibration to monitor the long term stability of the analog amplifiers.

The probe survival heater electronics is housed in the MAG electronics on a separate slice and is ground isolated from the rest of MAG both in the electronics and at the probe to protect the spacecraft in the event of a malfunction in the MAG electronics. The sensor heater is powered independently of the rest of the MAG electronics to allow the heater to operate when MAG is powered off. Additional spacecraft protection is provided by hardware and electronic heater fuses in series. When the probe temperature falls below –15°C the heater generates a pulse width modulated 50 kHz transformer coupled current to the 80 Ohm probe heater to maintain the probe temperature at –15°C. The maximum heater power is 400 mW at the sensor. During operation ~50 mW is dissipated at the sensor in the low field environment to be encountered during cruise and at Mercury. The sensor is blanketed by a double layer blanket so that the sensor dissipation and survival heater are expected to be sufficient to maintain the probe temperature at –15°C.

3.2.2 A/D Conversion

The analog outputs for the three axes are sampled simultaneously with three independent 20 bit Crystal 5508 sigma-delta A/D converters at a rate of 20 conversions per second. The useful resolution of the A/D converters is 18 bits. To ensure even time sampling, digital conversion is controlled by an on-board oscillator rather than synchronized to the spacecraft clock. Each axis is anti-alias filtered with a single pole low pass filter with a –3dB point at 10 Hz. The A/D converters apply an additional filter with a –3dB point at 17 Hz. The timing latency due to the anti-alias filters is 15.9 ms. The A/D conversion introduces a latency of 24.8 ms. The total intrinsic latency of the instrument was measured to be 42 ms. A self calibration is integral to the Sigma-Delta A/D converters which adjusts the conversion scale against a voltage reference when invoked by command. This A/D calibration invalidates the data for four conversion cycles.

In time series and frequency domain analysis it is crucial that the observations be uniformly spaced in time and since the MAG instrument uses on-board digital filtering it was essential that the sampling be uniform. For this reason the MAG samples are evenly spaced at 50 ms intervals driven by an oscillator internal to the MAG-EPU and are not synchronized to the spacecraft time. All three A/Ds are synchronized to the same sample trigger. The data are time tagged with the number of 50 ms ticks between the last 1-second spacecraft time pulse and the time that the A/D sample ready bit is set. Because the MAG-EPU clock and spacecraft clock have some relative drift, the MAG time tag slips slowly relative to the spacecraft resulting in an uncertainty of 25 ms in the precise time to which a given sample corresponds. The spacing between samples is however guaranteed to be uniform to within a microsecond. Recovering more precise timing tagging is possible by analyzing the time tags to establish the relative drift rate but is not necessary to meet the science objectives of the mission.

The 25 ms maximum error in the absolute time is well within the timing needs for MESSENGER science. The only other instrument with which MAG data will be correlated is the Energetic Particle Spectrometer (EPS) which has a minimum sample integration time of 0.5 seconds (for electrons). At 25 ms, the uncertainty in knowledge of the spacecraft position for a given MAG sample is 75 meters, corresponding to a maximum relative velocity of 3 km/s relative to the planet at perigee. At the minimum altitude of 200 km this corresponds to an angular uncertainty relative to a point on the surface at nadir of 0.02°, far smaller than the angular resolution to which the intrinsic field can be determined relative to external field sources [*Korth et al.*, 2004].

Protection from MAG A/D latch-up is passive. The A/D converters are the same as used on the magnetometer for NEAR-Shoemaker. Extensive latch-up automatic reset circuitry was used for NEAR-Shoemaker but was never activated in four years of magnetometer operation [*Lohr et al.*, 1997; *Anderson et al.*, 2001]. Since MESSENGER is a mapping mission rather than an event driven mission and given the experience that A/D latch-up with this converter was rare, for MESSENGER a passive latch-up protection was used eliminating the automatic reset circuitry. Reset is accomplished by powering the instrument off and on by command. Should latch-up occur, the latched A/D will be unharmed but will cease to execute conversions until power cycled, the data will be invalid and an A/D error bit is set. Samples of MAG A/D conversions and A/D status flags are included in spacecraft housekeeping monitored by operations so that a corrective MAG power cycle can be invoked promptly, potentially during the ensuing ground contact, to recover normal operations without significant loss of data.

The LVPS provides eight 14 bit A/D channels that are converted once per second. These are used to monitor the probe and electronics temperatures and the electronics current and forwarded to the EPU. Since extra channels were available, the analog signals for the three MAG axes are also sampled by these converters. Should any permanent problem develop with a science A/D converter, the LVPS data path can be promoted to recover the primary science observations. The resolution offered by the LVPS converters corresponds to 0.4 nT in fine range, eight times coarser than the data output by the MAG digital processing, but still sufficient to achieve the primary science objective for MAG. The gains of the LVPS A/D converters are monitored relative to the science A/Ds via the analog calibration signal.

3.2.3 Digital Logic and Processor

Instrument operation and modes are controlled and to a large extent implemented digitally in the EPU. The EPU uses a RTX2010 processor which is a 16-bit processor running at a nominal clock speed of 6 MHz. Field Programmable Gate Array (FPGA) Actels (Figure 6) are used for many hardware functions, including watchdog timer, Universal Asynchronous Receiver/Transmitter (UART) logic, and as an interface to the MAG electronics for data collection and instrument control. The MAG software interfaces with the MAG electronics via memory mapped I/O for data collection, range control, and electronics calibration. The MAG EPU communicates with the DPU via a 38.4 KBaud RS422/UART interface. The EPU has watchdog circuitry which times out if it is not reset in 5.6 seconds. Under normal operations the EPU software resets the watchdog timer once per second. If the watchdog circuit times out indicating abnormal MAG operation, an EPU reset is triggered and an alarm is sent to the DPU which reports to the spacecraft main processor (MP) where error counters are updated and a decision to turn the magnetometer off may be made under autonomy control. Range control is performed in the EPU based on data from all three science A/D converters and can be either automatic or commanded. The range selection is made by setting the discrete logic line to the analog electronics.

The interfaces between the DPU and MAG electronics are controlled by interrupts which the EPU software services. A time synchronization interrupt is issued by the spacecraft clock at precise one second intervals, less than 5 nanosecond jitter, corresponding to the start of the current mission elapsed time (MET) second. The precision of this time interrupt is limited by the EPU clock rate to 0.7 μsec, more than accurate enough to satisfy MAG science requirements. This is used to set the MAG time tag to record the time of magnetometer samples relative to MET to a resolution of 50 ms. The MAG EPU also supports a 38.4 KBaud RS422/UART interface between the DPU and the MAG EPU. UART interrupts are used to signal MAG to read a command from the DPU and to signal that the DPU is ready for data transmission from the MAG. The MAG EPU interfaces with the LVPS via an I2C counter timer interrupt to collect MAG probe temperature, electronics temperature, MAG DC/DC current and 3-axis magnetic field samples. This interrupt occurs once per second. An internal MAG clock drives the A/D conversion at 20 Hz and the A/D conversion data ready signal is sent to the EPU as an interrupt every 50 msec. Each sample consists of an echo of the commanded state of the magnetometer and the counts for each axis. The echoed command bits reflect the state of the magnetometer (analog calibration on/off, A/D calibration on/off, and range setting) when the field sample was taken. The first four interrupts are common to all instruments and perform absolute timing, command and data handling, and LVPS interface functions.

4. Instrument Software

4.1 Software Overview

The MAG software orchestrates data and command interface between the DPU and MAG, performs several data processing tasks and controls autonomous instrument operation. The command and spacecraft interface functions include receipt of MAG commands from the DPU and implementation of these actions in the instrument, receipt of spacecraft time and calculation of associated time tags. The software also handles transmission of the instrument state, health and safety data, science data telemetry and turn-off requests to the DPU. Data processing tasks performed by the software consist of digital filtering to accommodate a range of sampling rates, 1 to 10 Hz band-pass fluctuation amplitude calculation, data compression and science data formatting with header information into Consultative Committee for Space Data Standards (CCSDS) telemetry packets. Autonomous instrument operation controlled by the software includes range control, burst data triggering and fault detection. Each of these processes is described below.

MAG uses the FORTH language. A set of common routines are used for EPU-DPU interface, LVPS interface, CCSDS packet generation and data compression. Many elements of the MAG code, including the digital filtering, range control, and variable sample rate implementation were originally written for the NEAR-Shoemaker magnetometer [*Lohr et al.*, 1997]. New features used for MESSENGER include data compression, burst data collection including pre-burst buffering and LVPS A/D backup data acquisition. All features of the code were subjected to extensive testing to independently verify proper functionality.

The MAG EPU memory is organized in thirteen blocks or pages of 64 Kbytes and is allocated as follows. One page is reserved for boot Programmable Read-Only Memory (PROM), four pages of Electrically Erasable Progammable Read-Only Memory (EEPROM) are available for code, macros and tables, and eight pages of Static Random Access Memory (SRAM) is available for run-time code, macros and data buffers. The SRAM is allocated as follows: one page each for run-time code, macros, data buffer, telemetry buffer, and burst data buffer. Three SRAM pages were not used.

4.2 Instrument Control

4.2.1 Commanding

The MAG software controls the MAG electronics via memory mapped I/O. The MAG software sends a command from the EPU to the magnetometer electronics by writing a sixteen bit command word to an output register that controls the instrument via the FPGA. Commands sent to the magnetometer instrument perform the following functions: select the analog electronics gain state or range; invoke an A/D calibration cycle; and turn the analog calibration signal on or off. All other functions including the output sample rate, autonomous range control logic and various parameter settings for EPU processing are performed in digital processing by the EPU. To ensure that the instrument range and sampling rate are the same for all samples in every standard science packet and that the data within a packet are strictly evenly spaced in time, any command that changes the range, sampling rate or interrupts the sampling spacing (e.g. the A/D calibration) are acted on at the end of the science packet being collected when the command is received. A terminate science packet command is provided to truncate the current packet enabling prompt execution of commands that would otherwise be delayed.

4.2.2 Range Control

The instrument range can be controlled in automatic or manual mode. In manual mode, the instrument range is set by command. In automatic range mode, the software compares the largest absolute value of the signed count values against the current range's full scale and adjusts the range if needed to maximize resolution while keeping the readings on scale. On startup, the range is controlled in automatic mode and the default range is 0 or 'fine' (±1,530 nT full scale). The range control processing is the first action taken when a new sample is received by the EPU. The software evaluates the absolute value of the signed X, Y and Z counts. The maximum absolute value, S, is then compared against the full scale count value for the current range. If the current range is 0 and $S > 95\%$ of full scale for $N_{\text{to\_coarse}}$ consecutive samples then the range is changed to 1 or 'coarse' (±51,300 nT full scale). The default value for $N_{\text{to\_coarse}}$ is 1 so that the instrument immediately shifts to coarse range if the reading in fine range is larger than 1,473 nT. If the current range is 1 (coarse) and $S < 2.5\%$ of full scale or 1,266 nT for $N_{\text{to\_fine}}$ consecutive samples, then the range is changed to 0. The default value for $N_{\text{to\_fine}}$ is 1200 so the field must remain below 2.5% of coarse range full scale for one minute before ranging down to fine range. Note that 1,266 nT is 81% of full scale in fine range, well below the transition point to coarse range ensuring that an immediate transition back to coarse range is extremely unlikely. Both $N_{\text{to\_fine}}$ and $N_{\text{to\_coarse}}$ can be uploaded by command. If the automatic range control algorithm changes the MAG range, the current science record packet is closed and a new packet with a new header reflecting the new range is started with the first sample in the new range. The number of samples in a packet is given in the packet header.

4.2.3 Internal Calibrations

Two internal calibrations are available and are exercised by command. The first calibration monitors the analog outputs of all three axes. The analog calibration circuit injects a known bias current, determined by a reference voltage, into the analog electronics amplifier of each axis, simulating a magnetic field offset of one quarter the full scale value in each axis. Analog calibration is controlled by commanding the calibration signal on and off via a memory output register bit. Analog calibration is off at instrument turn on.

The second calibration is a self-calibration of the A/D converters. This is invoked by setting a specific output register bit high for two conversion cycles (to ensure that the A/Ds capture the calibrate signal). The A/D calibrate output register maps directly to the A/D internal calibration trigger of all three converters. This calibration takes two 1/20$^{\text{th}}$ second conversion cycles and the A/D produces no data during this time. To ensure that only valid data is read from the A/Ds, four 50 ms samples are dropped, which is reflected in the MAG time tag. The MAG software turns the A/D calibration off automatically (no command is needed) after calibration is complete. One A/D calibration is performed on startup.

The A/D calibration is the single exception to strict even internal sampling. Because of the interruption of the data collection, A/D calibrations are only allowed between science data packets and are not allowed during bursts (Section 4.4). Moreover, an A/D calibration flag is set in the instrument housekeeping for the packet immediately following the A/D calibration. The digital filters are also re-set and require a few seconds to settle. For this reason, A/D calibrations are planned to occur only with the instrument in its highest sample rate (no digital filtering used) and at points of the orbit of least interest (highest altitude and in the solar wind).

4.3 Data Processing

Magnetic field data are processed as follows. Every 50 ms when the A/D data ready flag is set, the EPU retrieves one unsigned 20 bit value for each axis from the digital electronics slice via the ACTEL gate arrays. If digital filtering is enabled, the EPU software converts the data to signed 32 bit values, scales the values to nT and removes fixed offsets before applying digital filtering commensurate with the commanded data output rate. The scaling and offset removal are performed to ensure that the filtering works across range changes which may occur automatically. After any necessary filtering and sub-sampling, described below, scaling corrections are removed and the data are rounded to 16 bit resolution. The data are then assembled into packets of 200 vector samples. If compression is enabled, the data are compressed using differential pulse code modulation (DPCM) compression, also known as FAST because it decompresses quickly. In DCPM as applied to the MAG standard science packet data, the first sample is retained in full and the remaining 199 samples are differences from the previous value. The number of bits used for the difference values is chosen to be the smallest that will accommodate the largest difference and is given in the packet header. The time tag for the first sample in the packet is the MET time in seconds for the first sample together with a counter giving the number of 1/20th second intervals of the first sample in the packet from the immediately previous MET second boundary. The packet header includes the time tag for the first point, a compression ON/OFF flag, the number of bits used for difference values if compressed, the sampling rate, number of samples and an instrument range flag. The header, up to 200 vector data and 1-10 Hz fluctuation amplitude values (discussed below) are assembled in a CCSDS telemetry packet and forwarded to the DPU which forwards them to the spacecraft solid state recorder (SSR). This data stream is the MAG standard science packet. An uncompressed science packet is 11.3 kbits corresponding to 56.5 bits per sample.

To accommodate variable telemetry allocations during the mission, MAG supports a range of sampling rates that are selected by command (Table 1). The available data rates in samples per second are 0.01, 0.02, 0.05, 0.1, 0.2, 0.5, 1, 2, 5, 10 and 20 and are denoted rates 0 through 10, respectively. If digital filtering is enabled and the commanded rate is 0.5/s or lower, the software applies a 0.5 Hz low pass filter and sub-samples the data to the commanded rate. For rates of 1, 2, 5 or 10/s the data are filtered using an IIR Butterworth low pass filter corresponding Nyquist frequency, 0.5, 1, 2.5 and 5 Hz, respectively. Section 5.3 describes the digital filters' frequency responses. For the 20/s rate no digital filtering is applied. Filtering can be commanded on or off for diagnostic purposes but is normally on. To prevent round off error propagation five bits of zeroes are added to each of the 20 bit adjusted 3-axis values before they are passed through the filter. After filtering, the scaling corrections are removed.

In addition to the vector samples, the software evaluates a 1 to 10 Hz band-pass average amplitude for one axis, selected by command. The average absolute value of the high pass filtered data is evaluated over one-second intervals. The result is scaled to counts to match the vector data count scaling. It is recorded as a logAC value with a 4-bit mantissa of the four most significant non-zero bits and a 4-bit power of two exponent of the 4th (least significant) bit of the mantissa. The logAC value provides a continuous monitor of the 1 to 10 Hz fluctuation level regardless of the commanded vector sample rate. It is included in the MAG high priority low rate housekeeping data (Section 4.4.1) to enhance orbital operations planning and is used internally to trigger burst data collection (Section 4.4.3). A logAC sample is created once per second and is included in the standard science packet at that rate or at the commanded science rate, whichever is lower.

4.4 Additional Data Products

In addition to the standard science data three other types of data are generated: low rate housekeeping, instrument status and burst. The low rate housekeeping data provides continuous monitoring of the instrument and low resolution data during periods of low link margin. The status data is contingency data of the instrument state that will normally not be downlinked but is available should a problem occur. The burst data provides internally triggered intervals of 20/s data during periods when the downlink rate does not permit continuous 20/s operations, that is, most of the time. This subsection describes each of these data and their acquisition control.

4.4.1 Low Rate Housekeeping Data

The instrument housekeeping data provides very low volume instrument health and safety monitoring and low time resolution vector and logAC samples. During operations at Mercury, downlink rates will vary with the Mercury-Earth distance and with the Mercury-Sun-Earth angle [*Santo et al.*, 2001]. When Mercury is close to the Sun as viewed from Earth, the link margin can be quite small. This results in a significant delay, two months or longer, between the time when standard science data is recorded on the spacecraft and when it is sent to Earth. During periods of low link rates, only low volume health and safety data will be down-linked with each daily contact. The housekeeping packet is the highest priority MAG data and will be down-linked on every pass during operations at Mercury to provide prompt data on instrument health and to facilitate observations planning by retrieving low time resolution full orbit vector and fluctuation amplitude data. The low rate housekeeping packet contains one set of probe and electronics temperatures and LVPS current readings, and ten vector magnetic field samples together with the corresponding ten logAC samples. Time tag and instrument range are included for each field sample. The time interval between field samples is commandable to either 50, 500 or 2000 seconds, the latter appropriate only for cruise. The housekeeping data is taken at the time of the first field sample in the packet.

4.4.2 Status Data

Instrument status data is acquired for examination in the event of unexpected instrument behavior. It consists of instrument command counts, instrument state (MAG circuitry calibration on/off, A/D calibration on/off, range control manual or automatic, software anti-alias filters on/off, manual range, actual range, selected AC axis, range change rate in the more sensitive direction, range change rate in the less sensitive direction, output sample rate, and compression on/off) electronics and probe temperatures, LVPS current, an A/D health monitor flag and samples of the magnetic field as recorded by the 14-bit LVPS A/D converters. The A/D health flag is set to one if all of the A/Ds are healthy. Otherwise this bit is set to zero. The LVPS A/D samples provide a back-up A/D conversion path with reduced precision in the unlikely event of a failure of one or more of the science A/D converters. In this event, the MAG status data priority will be promoted to the same level as the standard science data. The status data are acquired by the EPU once every second and recorded at any interval of one second or longer set by command. The time tag for status data is the 32-bit MET in the packet header and corresponds to the second in which the LVPS 3-axis sample included in the packet was collected.

4.4.3 Burst Sampling

A burst feature was included because the downlink rate from Mercury will not allow routine collection of 20/s data for long periods. Burst data consist of eight contiguous minutes of 20/s data. A burst collection is triggered when the 8-bit logAC value exceeds a commanded level. The axis to be used for this comparison is also set by command. The burst feature allows sampling of higher frequency signals during parts of the orbit and mission phase when high rate sampling is not possible throughout the orbit. By time windowing the burst intervals, the mode can be used to target specific regions of the orbit where boundary crossings or alternatively waves may be expected to occur but for which the appropriate trigger levels are likely to be quite different. Burst sampling is enabled or disabled via time tagged command. Burst collection is disabled on startup.

Magnetic bursts are initiated if the following conditions are met: burst collection is enabled (set by time tagged command), the instrument is in fine range, the logAC value exceeds the commanded trigger point, and the number of bursts allowed during the current burst window has not been met. The default burst limit and burst trigger level are set on startup to the following: burst limit = 1 and trigger level = 255. When a burst is triggered, the burst trigger logic is disabled and field data at 20/s are collected for a 480 second period, where the first 32 seconds of data is from the 32 seconds before the burst is triggered. The data is stored in SRAM memory page four and burst collection proceeds in parallel with other data collection. During a burst, A/D calibration is not allowed but there is no safeguard preventing an A/D calibration in the 32 second pre-burst interval. Eight minutes of 20/s data requires 57,600 bytes and so fits on one page of SRAM. At the end of the burst, the software compresses the burst data using a block size of 640 samples (32 seconds) and formats each data block in a telemetry packet. A complete burst interval is 9600 samples long so the entire burst data is sent via fifteen telemetry packets to the DPU. The MET and the five bit time tag for all the burst data packets generated for a particular burst are the same and correspond to the time tag, to 50 ms resolution, of the last sample in the burst. Time tagging the last point was done to allow a continuously rolling 32 second pre-burst buffer. Data immediately following the burst are passed to the 32 second pre-burst buffer and a subsequent burst is triggered no sooner than 32 seconds after the previous burst. This ensures that consecutive bursts are contiguous in time without overlap.

Because burst data collection occurs in parallel with standard science and other data collection, it also provides a convenient way to acquire the 20/s data that is input to the digital filtering and logAC calculation. This feature was used extensively in pre-flight checkout to verify filter accuracy, time latencies and the logAC calculation. In flight it will also be used in instrument checkouts to verify that all filters are working properly.

5. Pre-flight Calibration and Testing

5.1 Gain and Orientation

The MAG gain calibration and sensor alignment tests were done in two stages. Absolute gain calibration and sensor alignment measurements were conducted at the NASA Wallops magnetics facility in coarse range. This facility consists of a set of 20-foot coils yielding a 3 foot diameter center zone with a field uniform to 0.005%, power control stability to better than 2 nT (verified to 0.5 nT during the tests) and alignment precision to $< 0.01^{\circ}$. A scalar magnetometer with 1 nT absolute accuracy was used to specify the field used for this calibration. Optical cubes on the test fixture for this test provided precision alignment knowledge of the sensor relative to the facility coil axes. The coarse range absolute calibration was transferred to the fine range using the JHU/APL magnetics facility.

5.1.1 Polarity Tests

The polarity of each axis was checked during instrument integration and following integration to the spacecraft. The simplest and most reliable method uses the fact that the vertical component of Earth's magnetic field is downward in the northern hemisphere, in particular in Maryland and Virginia where all integration tests were done. By recording the sign of the signal from each axis as it is aligned with the vertical provides confirmation of the polarity. Alignment need only be within roughly 20^o of vertical for this to be definitive, so this test is easily done handling the instrument by hand. The second approach, used both at the Wallops and JHU/APL magnetics facilities, consists of approximately nulling the field at the coil center, placing the sensor in the coil center with its axes approximately aligned with the coil axes, applying a bias field of known direction along each of the three coil axes, and recording the polarity of the instrument signal. The second procedure also allows verification that the polarity of the two ranges is the same. A final polarity test was performed after instrument integration to the boom and the spacecraft. This was done using a test magnet whose North magnetic pole was known and aligning it so that its N-S axis was approximately aligned with one of the MAG axes and orienting the test magnet so that the S pole is closest to the MAG sensor, that is, the field along the axis of the test magnet points from the MAG sensor to the test magnet. The polarity of the MAG sensor as integrated with the boom and the spacecraft was confirmed to be as designed, that is, such that it will correspond approximately (see Section 5.1.3 below) to spacecraft coordinates following boom deployment.

5.1.2 Absolute Calibration and Relative Alignment

The technique used to provide absolute calibration and precise relative orientation of the three axes consisted of applying +50,000 nT (50,008 nT measured) in one direction and rotating the sensor in steps of approximately 45 degrees around each of the sensor's three axes. A total of 27 vector measurements were obtained (repeating the starting position for each axis). This procedure was repeated for a field of +10,000 nT (10,001.5 nT measured). Because the applied field is identical for each sensor orientation, the technique provides a precise correlation between both the gain and the orientation of the sensor axes. The gains and relative orientation are determined by using the fact that the magnitude is the same for all orientations. Denoting the counts in the X, Y and Z axes by c_x, c_y and c_z and the fixed offsets as c_{x0}, c_{y0} and c_{z0}, one writes the magnetic field in sensor coordinates as

$$\begin{aligned} B_x &= k_x(c_x - c_{x0}) \\ B_y &= \alpha k_x(c_x - c_{x0}) + k_y(c_y - c_{y0}) \\ B_z &= \beta k_x(c_x - c_{x0}) + \gamma k_y(c_y - c_{y0}) + k_z(c_z - c_{z0}) \end{aligned} \tag{1}$$

where k_x, k_y and k_z are the gain coefficients for each axis and α, β, and γ measure the contributions of X in the Y axis (α), X in the Z axis (β), and Y in the Z axis (γ), respectively. Because the applied field, B_{appl}, is the same for all orientations of the sensor, the six parameters are constrained by the residual

$$\Delta^2 = \frac{1}{N}\sum_i \left(B_{x,i}{}^2 + B_{y,i}{}^2 + B_{z,i}{}^2\right) - B_{appl}{}^2 \tag{2}$$

The fine range gain factors were determined by measuring the fine range response relative to the coarse range using the 2-meter coil system at JHU/APL. The APL magnetics facility provides a 2-foot diameter zone in which the field is uniform to 0.01%. The current control system is linear to 0.01% and provides 1-2 nT stability. The absolute accuracy is about 0.5% so this facility was not used for absolute calibration. With the sensor in the coils operating to approximately null the background field, a series of currents were applied to the facility coils to determine the response per unit coil current in coarse range. The range was then set to fine and another series of smaller currents were used to determine the signal response per unit coil current in fine range. The measured ratios of the scale factors between the two ranges were used to obtain the fine range scale factors in Table 2. The fine scale calibrations are accurate to 0.08%.

5.1.3 Sensor Orientation

The relative orientation of the sensor and an optical cube attached to the sensor housing was determined at the Wallops magnetics test facility by applying a field in the X-Z sensor plane and rotating the sensor to precisely align with an optical sensor. The ratio of X and Z fields then yields the angle of the sensor axes relative to vertical (or horizontal). After integration to the boom and with the boom deployed (vertically) the orientation of the same optical cube was measured relative to a cube on the root hinge. In final spacecraft alignment tests the root hinge orientation was determined. The final result is that the X-Z spacecraft axes are rotated 0.1^o clockwise (right handed) looking toward the +Y side of the spacecraft relative to the X-Z magnetometer sensor axes. The conversion for this azimuth orientation to spacecraft from magnetic sensor coordinates is

$$\begin{aligned} B_{x-sc} &= 1.0000 B_{x-mag} + 0.0017 B_{z-mag} \\ B_{z-sc} &= -0.0017 B_{x-mag} + 1.0000 B_{z-mag} \end{aligned} \qquad (3)$$

This conversion only accounts for the orientation in azimuth about the Y axis. The final orientation conversion from sensor to spacecraft coordinates will be determined from data acquired in-flight as described in Section 7.1.1.

The Earth fly-by which is afforded by the August 2004 launch provides the only post-launch opportunity to verify the azimuth orientation. It also provides an independent confirmation of the elevation orientation. Comparison with Earth field during fly-by encounters provides orientation accurate to 0.1^o by comparing the measured vector field to well known Earth model fields and has been done previously [*Anderson et al.*, 2001].

5.2 Instrument Offsets

The instrument offset was determined by flipping the sensor during the Wallops calibration. A small field was established in the facility and the sensor was then rotated 180^o and back to an accuracy of 5^o. The response of the two components in the plane of rotation was recorded. This measurement was repeated for two orientations to measure the offsets in all three axes. Since the instrument offset rotates with the sensor, the average of the output for the two orientations gives the offset. The precision of the 180^o rotation is not critical since even a 5^o error only introduces a 0.4% error in the offset. The offsets in the coarse and fine ranges were found to be identical to within the coarse range resolution. Table 2 gives the offsets in coarse and fine range in counts.

5.3 Frequency Response

The frequency response of the analog section of the instrument is determined by the low pass filter applied to the amplifiers' outputs and the additional low pass filter of the A/D converters. The left panel of Figure 7 shows the attenuation of the combined low pass and A/D filters which together yield a –3dB point at 11.1 Hz and attenuation of 17 dB/octave at 15 Hz (26 dB/octave at 20 Hz). The filter characteristics for the analog filter and the digital low pass filters are given in Table 3 and the right panel of Figure 7 shows the 1 Hz low pass IIR filter response (solid circles) together with the 1 Hz high pass IIR filter (open circles) used to evaluate the 1 to 10 Hz fluctuation amplitude. The high pass filter has its –3dB point at 0.87 Hz and attenuation of –75 dB/octave below 0.7 Hz.

5.4 Timing

5.4.1 Relative to Spacecraft Absolute Time

The MAG samples are time tagged to 50 ms using an internal clock that counts the number of 50 ms intervals since the last time pulse, PPS, from the spacecraft DPU. On average the time tag is 25 ms behind since if a square-wave jump occurs any time two A/D conversions, it is tagged no sooner than 50 ms after the previous conversion. Other fixed latencies are introduced by the characteristic response time of the fluxgate and by the analog anti-alias filter and in the A/D converters. The combined latency was measured by using the PPS signal to trigger a square wave signal which sourced a current to a test coil placed around the MAG sensor in a low field environment. Over a period of hours, the DPU emulator clock and the MAG EPU clock drifted by more than 50 ms so accumulating data over many hours, provided a statistical sample of the appearance of the leading edge of the square pulse in the MAG data. If there were no instrument latency the average delay of the square wave leading edge would be 25ms. However, the average leading edge was delayed by 67 ms relative to the PPS indicating an instrument delay of 42 ms. The expected instrument latency is in excellent agreement with this value. The anti-alias filtering (15.9 ms time constant) and the instrument feedback response (time constant of 3.2 ms) in series account for 16.3 ms. The A/D conversion time is 49.5 ms corresponding to a latency of 24.8 ms. The expected instrument latency is the sum of 16.3 ms and 24.8 ms or 41 ms.

5.4.2 Filtered Data

Digital filtering introduces additional latency relative to the 20/s data. The digital filters are Butterworth IIR filters with their –3 dB points set for the corresponding sampling rate (e.g. 0.5 Hz for 1/s sampling or rate #6) as shown in Table 3. Rates 0 through 6 are sub-sampled from the 0.5/Hz filtered time series and all have the same time lag. Rates 7, 8 and 9 have different digital IIR filters and correspondingly different lag times. Rate 10 is not digitally filtered and is lagged by 42 ms. The time lags are given by the properties of the digital filters and were confirmed in testing by acquiring filtered and burst data simultaneously. Since the burst channel data is the native 20/s data, comparison of these data against the filtered data allows direct confirmation of the lag introduced by the digital filter. The lags obtained in this way were accurate to 1 ms (3-sigma) and agreed with the theoretical values. The net time lag including both the instrument and digital filter time lags are given in Table 3. The physical sample times are obtained by subtracting the net lag from the time tags reported in telemetry.

5.5 Environmental Testing

The sensor and electronics were tested prior to integration on the spacecraft in vacuum over a wide range of temperatures to ensure functionality throughout the possible range of environment encountered at Mercury. The sensor temperature range used was –106°C to +47°C and the electronics temperatures ranged from –44°C to +63°C in repeated cycles and in all combinations of warm and cold sensor and electronics. Instrument performance was monitored throughout thermal/vacuum testing in both ranges by exercising the A/D calibration and the analog calibration feature in both ranges. Fine range operation was achieved using cancellation coils located near the sensor in the test chamber that reduced the field at the sensor to less than 1% of the ambient field. The resonant drive circuit remained operational throughout the complete range of sensor and electronics temperatures. Analog electronics drift was characterized using the internal calibration and for the fine (coarse) range was 22 (16), 35 (35) and 11 (20) ppm/C^{o} in X, Y and Z, respectively. This small drift ensures variation in the analog gain of less than 0.1% over the expected operating electronics temperature range, 0^{o}C to 30^{o}C. The relative alignment of the three axes and the gain were tested at the JHU/APL facility before and after environmental testing and were identical to within the accuracy of the measurements, 0.08% in gain and 0.03^{o}.

5.6. Spacecraft Magnetics

All components of the spacecraft employing magnets or magnetic materials were screened for magnetic signatures. In addition, uncompensated current loops were avoided in the design of the battery, solar arrays, power distribution system and spacecraft harness. The three spacecraft systems that employed magnets or magnetic materials presenting the greatest risk to the magnetometer were, in decreasing order of significance, the propulsion latch valves, the momentum reaction wheels, and the battery cells. The steps used to mitigate these sources of contamination are summarized in this section.

5.6.1. Fixed Spacecraft Field

The magnetic moment of each latch valve of the propulsion system was characterized prior to assembly of the propulsion system to 1% accuracy at the JHU/APL magnetics facility. The geometry of the propulsion system was then used to construct a mathematical model of the propulsion system field and estimate the field at the deployed magnetometer location. This model was tested against measurements of the magnetic field of sub-assemblies of the propulsion system and found to be consistent with the measurements to within the ~20% noise level of the measurements (due to the magnetic contamination of a conventional work area at the propulsion system vendor). This level of accuracy is more than sufficient to demonstrate that the model was free of gross errors (e.g. sign errors). A pair of cancellation magnets was then designed to cancel the propulsion system field at the deployed sensor location. The cancellation magnets were attached to the spacecraft structure early in integration.

The battery cells use Nickel in both the casing and in the active elements of the battery. The cells were demagnetized using a solenoid degausser in an ambient field less than 0.5% of Earth's field at the JHU/APL magnetics facility. This reduced the residual magnetic moment of the cells by roughly a factor of ten from their moments as delivered from the manufacturer. Numerous other spacecraft components were demagnetized to minimize their contribution to any spacecraft residual field. These included: stainless steel hardware required for the phased array antenna, solar array interconnects (after delivery of the solar arrays using a hand demagnetizer) and stainless steel 'velcro' fastening material for the spacecraft sunshade.

The fixed residual spacecraft moment of the spacecraft was assessed near the end of spacecraft integration by means of a pendulum test in which the spacecraft was suspended from an overhead crane, displaced two feet horizontally from vertical at the payload adapter fitting (bottom) by pulling laterally at the bottom of the adapter fitting. Releasing the spacecraft provided a clean pendulum motion without stressing the spacecraft structure. The magnetic signature of the spacecraft was monitored simultaneously with three test magnetometers. This test confirmed that there were no magnetic field sources other than those identified above: the only detectable sources were due to the combination of the propulsion valves and compensation magnets, consistent with the net field expected from the magnetic field model developed for the propulsion system modified to include the cancellation magnets. Determination of the spacecraft field in-flight is discussed in Section 7.1.2.

5.6.2 Variable Spacecraft Field

Early in spacecraft development the momentum wheels were found to yield signals larger than 0.3 nT at the deployed sensor location. The source was identified as a magnetic moment rotating with the rotor. Demagnetizing the steel in the rotor and bearings reduced the magnetic signature by a factor of three or more. An additional factor of three was obtained using a single layer of 0.8 mil thickness magnetic shielding. All wheels were tested with magnetic shielding to ensure that they produced less than 0.03 nT at a distance of 4 meters. The shielding mass for each wheel was 33 g. Tests during integration confirmed that the magnetic field from the wheels was less than 10 nT at distances from the wheels of less than 20 cm.

Magnetic fields generated by the power system were also minimized. The solar arrays were backwired, that is, the power return for each string was routed along the back of the panel to retrace the cell string on the front face. In addition, adjacent strings were arranged with reversed polarities to approximately cancel the moment due to the string-backwire loop. The power system harness used twisted pair power/return lines. All sub-system power returns were routed back to the power distribution electronics in twisted pair with the corresponding positive power lead. Special attention was also paid to the MESSENGER Laser Altimeter (MLA) instrument which includes high current electronics to drive the laser pulses. Loop cancellation designs were used within the power distribution electronics as well. Finally, the battery cells were wired in a figure eight pattern and the orientations of the cells fine tuned to ensure that the moments transverse to the cells' axes also cancelled. The battery moments both static and when charging/discharging were measured in pre-integration tests. The charging/discharge moment was verified to be dominated by the quadrupole moment out to a distance of one meter. Test measurements and design calculations indicate that the field at the deployed magnetometer from the solar arrays and battery current loop will be less than 20 pT.

Variable spacecraft fields were monitored with the flight magnetometer in its stowed configuration while spacecraft systems were tested during spacecraft integration and environmental testing. To maximize the sensitivity of these tests, the coil system used for MAG environmental testing was used to allow MAG operation in fine range. The background noise levels during these tests ranged from one to several nT. No signals associated with the momentum wheels were detected at a level of 1-2 nT. In addition, no signal was detected when the battery changed from charge to discharge state confirming that the battery layout design was successful. The only signal identified in the stowed flight magnetometer data was a 20 nT step associated with a propulsion tank heater within 30 cm of the stowed MAG sensor. This corresponds to a field of less than 0.02 nT at the deployed MAG sensor. To search for possible dynamic magnetic field sources with greater sensitivity, additional measurements were made with a portable test magnetometer that was positioned close to the subsystem of interest. Such measurements were made of the reaction wheels, power distribution system, solar array drive motors, and other systems and revealed no magnetic signatures at a level of 10 nT at a distance of 10 to 20 cm, consistent with a field at 3.6 meters of less than ~2 pT.

6. Flight Checkout & Performance

6.1 Turn on and Initial Checkout

MESSENGER was launched at 2:16 AM EDT on 3 August 2004 and nine days later the MAG instrument was turned on for initial checkout. Figure 8 shows the first data returned after MAG turn on including an initial checkout (note that 5000 counts corresponds to approximately 235 nT in fine range). At turn on the instrument remained in its sensitive range since the baseline field in the stowed position was well within fine range full scale. The baseline field in the stowed configuration was approximately 7000 counts (300 nT) in X, –5000 counts (235 nT) in Y, and 2000 counts (95 nT) in Z consistent with expectations for the stowed sensor location since the sensor is close to propulsion latch valves and thrusters on the spacecraft –Z deck. The initial checkout consisted of commanding the instrument to coarse range, activating the analog calibration twice, commanding to fine range and again activating the analog calibration twice and returning to auto-ranging mode. The instrument performed exactly as in pre-launch testing. The analog calibration steps were within 0.1% of pre-launch values on average (0.26% worst case) indicating no significant change from pre-launch testing.

6.2 Stowed Measurement of Spacecraft Variable Fields

Data obtained with the sensor in the stowed position are very valuable for assessing variable spacecraft magnetic fields. Because the spacecraft initial cruise phase carries the spacecraft slightly beyond 1 AU heliocentric distance, the spacecraft sun shade (Figure 1) was turned away from the sun to keep the spacecraft systems warm without using excessive power. To avoid risk of partial solar array shadowing the MAG boom remained stowed during this phase of cruise. This provided an opportunity to acquire magnetic field data for a variety of spacecraft systems and instrument checkout activities to verify that the variable spacecraft magnetic fields were small. Figure 9 shows a segment of data from 12 August 2004 together with spacecraft power system data. Two features are evident in the Z-axis data (red trace) and were similar to those in the X and Y axes: a quasi-periodic square wave with a 400 count (~20 nT) amplitude; and a beating signal with maximum peak to peak amplitude of 30 counts (~1.5 nT). During this time interval two instruments performed their initial activation/checkouts, the Neutron Spectrometer (NS) and the Gamma Ray Spectrometer (GRS). Their instrument currents are shown by the green and blue traces, respectively. The current to the primarily propulsion Helium tank heater is shown by the solid track and the dashed trace shows the primary spacecraft survival heater. Because the spacecraft system uses analog multiplexing to sample the power system currents and since the spacecraft survival heater is sampled immediately prior to the Helium tank heater, there is a slight residual of this current in the Helium tank heater current reading. The 20 nT square wave is clearly due to the Helium tank heater current as expected since this signal was observed in spacecraft level testing prior to launch. The other heater current, though larger is not evident in the MAG data. No step signals occur at when the currents to NS and XRS change.

The beat pattern signal in Z was not identified in pre-flight testing owing to the 1-2 nT environmental noise during these tests. Figure 10 shows a close up of this signal and Figure 11 shows ~3 seconds of data during a beat maximum. The signal is a 1.5 nT peak to peak beat. This signal shows up very clearly in the AC channel data which provides a convenient means of measuring the beat period. This period was very stable at near 1,090 seconds indicating a source with a stable frequency of 10 Hz to within one part in 10^4 as measured against the MAG internal clock. By monitoring the change of this beat period when the spacecraft timekeeping was tested on the precision and coarse oscillators it was confirmed that the signal is synchronized to the spacecraft clock. The amplitude of the signal approximately doubled when both star cameras were operated (normally only one star camera is on) confirming that star camera image capture, which occurs at 10 Hz and is synchronized to the spacecraft clock, is the source of this signal. The star cameras are mounted on the –Z deck and are located less than 20 cm from the stowed MAG sensor (cf. Figure 1). This signal will be well below a few pT after the MAG boom deploys.

The residual higher frequency noise of the spacecraft can be estimated from the data in Figure 10 by the 'thickness' of the two bands that comprise the beat signal. This noise is about 5 counts or 0.25 nT even when the reaction wheel spin rates are all within the 10 Hz low pass band of MAG confirming that the demagnetization and magnetic shielding successfully eliminated contamination signals from the reaction wheels. Note also 0.3 nT step at 837,900 MET which is attributed to another thermostatic heater. The 0.25 nT noise is attributed to other spacecraft sources which have not been identified but will be reduced well below the MAG resolution after boom deployment.

Operations of other spacecraft systems and instruments have been monitored throughout early operations and the only signals comparable to or larger than the Helium tank heater signal identified to date are due to a heater on the nearest phased array antenna (within 30 cm of the stowed MAG sensor, cf. Figure 1) and operation of the propulsion system valves. Magnetic field monitoring will continue after MAG boom deployment during spacecraft maneuvers and instrument operations to verify the magnetic cleanliness at the deployed location. All of the observations to date are consistent with a variable spacecraft field noise below the digitization resolution of MAG after deployment.

7. Observation Strategy and Plan

7.1 In-flight Calibration Activities

There are a variety of activities that will be conducted after boom deployment to characterize the residual spacecraft magnetic field at the deployed sensor location, to establish the precise sensor orientation and to validate coordinate transformation software.

7.1.1 Pre-deployment Monitoring

More than six months of data have already been acquired with the MAG boom stowed corresponding to numerous spacecraft checkout activities. Analysis of these data is ongoing and includes characterization of signatures from all payload subsystems, propulsive maneuvers and system checkout/test activities. The purpose of these analyses is to identify those signatures if any that would contribute to the measurements after deployment. The present state of analysis indicates that only the action of thrusters and magnetic latch valves of the propulsion system will generate signatures detectable post-deployment. There is no requirement to conduct science observations during propulsion events. The compensation magnets were chosen to compensate the field with the valves in their non-thrusting positions. It is anticipated that the pre-deployment data will be used to better characterize unanticipated signatures, if any are detected after deployment. Finally, MAG will acquire high rate data during the MAG boom deployment activities. These data will provide important confirmation of boom deployment and motion of the boom during deployment.

7.1.2 Interplanetary Observations

The science objectives for MAG require that the spacecraft residual field be known to within 1 nT. The magnetic compensation design should yield a residual field smaller than a few nT but this must be confirmed, characterized and monitored to assure that this contribution can be accurately removed. Two approaches will be used to determine the fixed field both of which have been successfully used in previous missions in interplanetary space. In the first, the spacecraft will be maneuvered to rotate about a known axis while the field is observed. For MESSENGER rotation about the Y-axis is the least stressful to spacecraft systems since this does not change the spacecraft orientation relative to the spacecraft-sun direction. This maneuver yields the spacecraft residual in the X and Z components. The results of this procedure are typically accurate to 0.5 nT or better [e.g. *Anderson et al.*, 2001]. To determine the Y-axis residual field requires rotating the spacecraft about either X or Z. Both of these involve off-pointing the solar arrays and exposing the back of the spacecraft to the sun which is not ideal because this not only exercises the spacecraft systems in ways for which they are not primarily designed but changes the magnetic state of the spacecraft. One X-axis rotation is planned prior to the Earth flyby. Depending on the experience and results with the X-axis rotation this may or may not be repeated.

The known properties of the IMF will therefore be used to complete the Y component residual field determination. On time scales of hours and days, variations in the IMF are predominantly rotational and these natural fluctuations can be used to identify the zero point of the field by identifying a fixed vector offset in the measurement which yields a field that is on average orthogonal to the fluctuations. In addition, the vector average of the IMF tends to zero on time scales of many solar rotations (27 days). Thus, using long term continuous observations, one can use both the rotational characteristics of the IMF and the long term averages to identify the 'zero' point of the IMF which in turn is the vector residual field of the spacecraft. Combining these determinations with the X and Z residual determinations from the rolls and the Y residual estimates from the flips allows a robust determination of the spacecraft vector residual field. Analysis identical to this approach used on Voyager, ACE [*Smith et al.*, 1998]) and NEAR-Shoemaker [*Anderson et al.*, 2001] gave residual field determinations accurate to <1 nT, sufficient for MESSENGER science requirements. Because MAG includes a 0.01/s rate corresponding to 0.56 bits per second, continuous sampling during cruise can be conducting to obtain the required long term IMF observations to support this analysis without burdening spacecraft operations.

The tilt of the sensor relative to the spacecraft Y axis must also be determined in flight. The elevation orientation is defined as the direction of the normal to the sensor X-Z plane relative to the normal to the spacecraft X-Z plane. Since this angle depends on the equilibrium points of both boom hinges, which in turn are likely to be slightly different in space than in ground testing, the elevation orientation is difficult to determine in pre-launch tests. In fact however, this orientation is accurately determined in-flight by taking magnetic field measurements while the spacecraft rolls about the Y axis. (The azimuth of the sensor about the Y axis was accurately measured in pre-fight and is not sensitive to the equilibrium boom hinge positions.) The elevation angle analysis uses the fact that the ambient IMF rotates in the spacecraft frame during the roll. While the rotating field appears primarily in the X and Z axes but some amplitude will generally appear in the Y axis. The amplitude of the roll signal in the Y axis relative to that in the X-Z plane gives the tangent of the angle between the sensor X-Z plane normal and the spacecraft X-Z plane normal. In addition, the phase of the Y roll signal relative to the X axis roll signal gives the azimuth of the sensor X-Z plane normal about the spacecraft Y axis. This technique has been used in interplanetary space on numerous missions including Voyager and NEAR and typically yields the sensor X-Z plane normal direction to accuracies of 0.1°, more than adequate for MESSENGER requirements.

7.1.3 Earth Flyby Observations

The mission design for the 3 August 2004 launch includes a gravity assist at Earth on 2 August 2005. The closest approach altitude of 2300 km ensures that the magnetic field will be large enough to provide a valuable validation check. To compare with Earth's field it will be necessary to transform the data into Earth fixed coordinates which is exactly analogous to the transformations required for Mercury analysis. The Earth flyby therefore provides an opportunity to validate that the coordinate transformations are implemented properly. The comparison also provides an independent check of the sensor orientation relative to spacecraft coordinates accurate to 0.1° by transforming a model field into spacecraft coordinates and comparing with the observed field [*Anderson et al.*, 2001].

7.2 Mercury Fly-by Observations

The three Mercury flyby maneuvers in the MESSENGER mission design provide unique opportunities to observe the equatorial regions of the planet at low altitude. During orbital operations the minimum altitude at Mercury's equator varies from ~900 km to ~1700 km, too high to resolve any smaller scale features that may be present. The flybys are the only opportunities in the mission to sample the equatorial regions at low altitude. Moreover, lower altitude data near the equator provides important constraints on the intrinsic field inversion [e.g. *Korth et al.*, 2004]. The flybys will all occur at altitudes of ~200 km, lower than the closest Mariner 10 Mercury encounter, and will significantly improve our knowledge of the planet's magnetic field prior to MESSENGER orbit insertion at Mercury because they will not only more than double the number of trajectories but they provide different cuts in body fixed coordinates. The additional longitude coverage is very important for constraining multi-pole inversions of the intrinsic field [cf. *Connerney et al.*, 1988].

7.3 Mercury Orbital Observations

The MESSENGER orbit around Mercury will be a 12.0 hour period eccentric orbit reaching a minimum altitude of ~200 km at ~80° N and having a maximum planetocentric distance of 7.6 R_m. Depending on the local time of the orbit, the spacecraft will spend about 1/3 to 1/5 of each orbit within Mercury's magnetosphere. Because characterization of the intrinsic magnetic field structure depends on a quantitative understanding of the magnetospheric structure and currents, the entire magnetosphere transits are important. In addition, the dependence of the magnetospheric currents on the local IMF mean that measurements when MESSENGER is in the solar wind will also be needed to help constrain the IMF conditions imposed on the system as much as possible.

The observation strategy is also determined by the downlink rate profile for the mission. Because the total telemetry volume for MESSENGER allocated to MAG is not large enough to allow continuous 20/s operation, MAG operations will be tailored to focus on the regions of greatest interest while still providing full orbit coverage at lower sampling rates. In addition, the telemetry downlink from MESSEGNER will vary considerably during orbit operations and there will be periods of very low downlink when Mercury is close to the Sun as viewed from Earth. The downlink variability implies that there will be periods months in duration when data will be stored on the recorder for later playback while only very low volume data will be available on a daily basis for safety monitoring. Observations during the orbital phase will be planned no less than two weeks prior to their execution. The low volume data must therefore be sufficient to allow intelligent observations planning prior to receipt of the standard science data. The MAG observations and data collection strategy is designed to provide full orbit coverage while offering high time resolution observations of regions of interest.

7.3.1 Low Rate High Priority Data

The low rate housekeeping data described in Section 4.4.1 above is the highest priority MAG data and will be telemetered daily even during periods of low link margin. During orbital operations these data will provide instrument health data (temperatures and current) every 500 seconds as well as vector magnetic field and logAC fluctuation level samples every 50 seconds (860 samples per orbit). These data will therefore provide prompt information on the instrument performance and recent observations. The burst capability is triggered by the logAC fluctuation level and will be used routinely to allow high time resolution observations of intermittent waves, substorm occurrence, or boundaries whose locations or timing cannot be accurately predicted. Because the fluctuation levels associated with these phenomena are not presently known and are likely to be variable, the logAC values are included in the high priority data to help identify the burst trigger levels appropriate to the local time and region of interest. The full orbit vector data will also provide necessary information on the locations of boundaries and their variability to identify the appropriate time windows during which bursts should be enabled and to identify time ranges during the orbit to be used for enhanced sampling rates in the standard science data.

7.3.2 Standard Science Data

The primary science observations are provided in the standard science data which consists of vector and logAC samples at the commanded rate as described above in Section 4.3. During orbital operations the rates used will be varied with spacecraft location in Mercury's magnetosphere or relative to boundaries. Early in the orbital phase the link margins will be high enough to support high resolution sampling throughout the orbit for a number of orbits, roughly ten. At other times the sampling rate will have to be tailored to the specific region of interest. In general, solar wind observations will be made at lower sampling rates and higher rates used closer to the planet. Sampling rates coarser than 1/s are not anticipated, except possibly in the solar wind. The logAC channel provides fluctuation levels down to 1 Hz so 2/s vector sampling is required to achieve complete frequency coverage. In general therefore, a minimum sampling interval in the magnetosphere of 2/s will be used both to ensure full frequency coverage and to provide sufficiently rapid pitch angle information to the EPS. Periods when the orbit crosses the sub-solar magnetopause will be targeted for higher time resolution sampling as will magnetotail neutral sheet crossings. Rates will be commanded using time tagged commands planned at least two weeks prior to the observations. The low rate housekeeping data will be used to assign the appropriate time windows to ensure that the regions of interest are successfully covered.

7.3.3 Burst Data Collection

The burst mode will be used to collect high rate vector data during portions of the orbit and/or during times of the mission when high rate sampling is limited. This will be implemented by selecting a time window during which burst collection is enabled. The time window would be selected to span the region of interest and the logAC trigger level selected appropriate to the target region. During periods of low downlink the low rate housekeeping data can be used to identify the appropriate logAC trigger level. On average one burst per day will be acquired.

8. Data Products

Timely access to data is important for instrument monitoring and observations planning. Science analysis requires additional information and processing. To support both planning and science analysis MAG data products are produced at several stages of the analysis. These include quick look and instrument status information, science analysis information and preliminary analysis products.

8.1 Quick Look and Instrument Status

The first step in processing is to read all of the packets of a given type, low rate housekeeping (LHK), standard science data (SSD) and status (STA) for a given day to generate a time ordered record of all samples of the corresponding type. The burst data (BST) is handled slightly differently. To prevent UTC day boundaries from dividing a burst, all fifteen 640 point packets for a given burst are converted into a single BST file. Time in these Experiment Data Records (EDR) includes MAG timing latency corrections but is retained in mission elapsed time (MET) to preserve independence in processing from updates to conversions from spacecraft time to UTC and to allow easiest correlation with other MESSENGER mission data and operations logs which are all ordered by MET. The EDRs are used to generate quick look plots to allow rapid assessment of the data and instrument status. To date, quick look plots for standard science data, low rate housekeeping and status data have been developed. No products have been developed for burst data since none of this data type have yet been acquired in flight.

Figure 12 shows examples of SSD (left) and LHK (right) quick look plots for day 315, 10 November, 2004. From top to bottom the SSD plot shows: the logAC counts and the AC axis (red trace, right hand scale, X=0, Y=1, Z=2); the instrument range (fine = 0, coarse = 1); the time increment between consecutive vector samples (black trace) and logAC samples (red trace); the X, Y and Z axis magnetic field values in counts. From top to bottom the LHK plot shows: the instrument current; the electronics temperature; the probe temperature; the instrument range; the logAC values; and the X, Y and Z axis magnetic field values in counts. The baseline values due primarily to the spacecraft field at the stowed position are not subtracted from these data. The field panels' scaling adjusts to the variation of each day's data but the data range is identical for all three field data panels. For this days' data each major division is 200 counts, ~10 nT. The LHK data for this day was sampled at 50 seconds for X, Y, Z and logAC (500 seconds for the current and temperatures). Comparing the logAC and X, Y and Z field data between the SSD and LHK data shows that the coarse time resolution provides an excellent overview of the data. The 20 nT (in Z) quasi-periodic signal from the Helium tank heater is clear and is about half as large in Y and essentially absent X. The logAC exhibits a spike whenever the heater turns on or off. A magnetic cloud associated with an interplanetary coronal mass ejection (ICME) was passing over the spacecraft during the first half of the day and the features of this event are clearly evident. At ACE the magnetic cloud field peak intensity was ~40 nT and lasted from ~1800 UT on 9 November to about ~1200 UT on 10 November. During this time MESSENGER was ~1.075 AU from the Sun and ~0.175 AU from the Earth and about 12^o to the east of Earth. The periodic signature in the logAC data is the star camera image capture interference signal which will go away when the boom is deployed.

Figure 13 shows corresponding plots for day 50, 19 February, 2005. For this day the IMF was much more quiescent as reflected in the lower variations, aside from the Helium tank heater signal which is was on much less owning to the fact that the spacecraft was now 0.97 AU from the Sun. The major division in the magnetic field data panels is 100 counts (5 nT) in these plots. In addition, the AC axis was changed to X from that for day 315 2004 when it was the Z axis. The logAC channel reads 1 or 2 counts (0.05 nT/count) indicating the low noise level of the spacecraft in this component at this time even in the stowed sensor location.

8.2 Calibrated Science Data

The first step in producing calibrated data from the EDRs is conversion to orthogonal coordinates and physical units using the calibration values in Table 2 and the formula of Equation (1). The data are then transformed into spacecraft coordinates using the azimuth correction in Equation (3) and the elevation orientation to be determined from the in-flight spacecraft roll maneuver (see Section 7.1.2). The residual spacecraft offsets are then subtracted, which are in turn determined from the spacecraft roll analysis and IMF statistics. (Because these steps require the results of in-flight calibration activities which cannot occur until boom deployment this processing will not be implemented until some time thereafter.) An intermediate product will then be generated consisting of the vector samples in physical units, transformed to spacecraft coordinates and with the spacecraft offset removed together with time in both MET and UTC. These data are in a form most useful for the EPS team. Time ordered files will be created from each daily or burst EDR file. In addition, the housekeeping data, instrument state (e.g. range, sample rate, AC axis) and burst status will be collected in a MAG activity/state log.

Because MESSENGER will transit a variety of regions and will address science appropriate to different coordinate systems, a next level product will be generated that will include spacecraft location and all relevant coordinate transformation matrices. Because the spacecraft location is essential in the subsequent analysis of magnetic field data, the spacecraft position relative to Mercury (or Venus or Earth as appropriate to each mission epoch) will be added to the magnetic field data in the form of the vector from the planet's center to the MESSENGER spacecraft in J2000 coordinates. In addition, coordinate transformation matrices will be evaluated and included. The first transformation required is from spacecraft to J2000 inertial coordinates and will be applied to the magnetic field data. Additional transformations will then be provided from J2000 to various physical systems including: Mercury-centered body-fixed, Mercury-centered magnetospheric, Mercury-centered solar wind, and heliocentric (appropriate for cruise). Magnetospheric coordinates depend on the orientation of Mercury's magnetic dipole as estimated by derived analysis products and will, therefore, be updated during the orbital phase of the mission. Corresponding coordinates for Earth and Venus will also be provided to support analysis of data acquired during these gravity assist maneuvers with these planets. All of these transformations are valid for both the magnetic field and the spacecraft position vectors.

All subsequent analysis products and displays will be generated using these calibrated data. The first of these are inversions for the planetary magnetic moment and higher order terms as discussed by *Korth et al.* [2004]. The results of these inversions will be used to update the Mercury magnetosphere coordinates and to calculate residuals of the measurements from the intrinsic field. The main field residual data are appropriate for calculating dynamic spectra of the burst and vector field data, identifications and logs of magnetopause and bow shock boundary crossings made in coordination with the EPS team and combined displays of the magnetic field and particle data. Pitch angle information will of course use the full magnetic field vector rather than the residual from the intrinsic field. The residual magnetic fields will be used to develop a semi-empirical magnetospheric model. As this model is refined it will be used to improve the corrections applied in analysis of the intrinsic magnetic field. Burst observations will be processed for spectral signatures of heavy ions and wave and turbulence processes in various areas of the magnetosphere. Analysis of these data will be event-driven and will be performed in close association with EPPS observations as will analysis of highly time-dependent signatures in the magnetic field.

9. Summary

The MESSENGER magnetometer instrument will provide accurate magnetic field measurements for the characterization of Mercury's magnetic field structure. The two range instrument provides coverage of fields up to ±51,300 nT in coarse range, resolution of 0.05 nT in fine range and full vector sampling up to 20/s. Pre-flight calibrations establish the absolute accuracy to 0.08% in the sensitive range (±15,300 nT). The instrument is tailored to the MESSENGER mission telemetry constraints to provide sampling rates from 100 seconds between samples (0.56 bits per second) to 20 samples per second (1130 bits per second) which is then compressed using a single point difference lossless algorithm. A 1 to 10 Hz bandpass amplitude channel provides continuous sampling of higher frequency fluctuation levels for observation planning and triggering of burst sampling when the telemetry rate does not allow continuous high rate sampling. MAG therefore provides maximum science return for intrinsic field studies and characterization of magnetospheric processes.

Success in meeting the observational objectives depends also on ensuring that contamination magnetic fields are minimized. The 3.6 meter long MAG sensor boom is shorter than booms used on previous spacecraft conducting high precision magnetometry so a detailed spacecraft magnetics program was followed that identified sources of fixed and variable magnetic fields early in the spacecraft development process and pursued design recommendations and mitigation steps. Design approaches included solar panel backwiring, use of twisted pair power and return wiring, single point grounding and wiring layouts of high current subsystems (battery and MLA) to minimize dipole current loops. Mitigation steps included cancellation magnets for the propulsion system components and magnetic shielding in combination with rotor and bearing demagnetization for the reaction wheels. Measurements during spacecraft integration and in flight prior to MAG boom deployment indicate that the variable field contribution from the spacecraft will be below the MAG resolution of 0.05 nT when deployed. The fixed spacecraft field is expected to be below a few nT. The MESSENGER magnetometer will therefore provide data to support accurate characterization of the intrinsic field, magnetospheric structure and dynamic processes throughout Mercury's magnetosphere and its boundaries with the solar wind plasma.

References

Aharonson, O., Zuber, M. T., Solomon, S. C., Crustal remanence in an internally magnetized non-uniform shell: A possible source for Mercury's magnetic field? *Earth Planet. Sci. Lett.*, *218*, 261-268, 2004.

Anderson, B. J., L. J. Zanetti, D. H. Lohr, J. Hayes, M. H. Acuna, C. T. Russell and T. Mulligan, In-flight calibration of the NEAR magnetometer, *IEEE Trans. Geoscience and Remote Sensing*, *39*, 907-917, 2001.

Burlaga, L. F., Magnetic fields and plasmas in the inner heliosphere: Helios results, *Planetary and Space Sci.*, *49*, 14-15, p. 1619-1627, 2001.

Christon, S. P., A comparison of the Mercury and Earth magnetospheres: Electron measurements and substorm time scales, *Icarus*, *71*, No. 3, 448-471, 1987.

Connerney, J. E. P., Ness, N. F., Mercury's magnetic field and interior, in Mercury (F. Vilas, C. R. Chapman, and M. S. Matthews, Eds.), University of Arizona Press, Tucson, pp. 494–513, 1988.

Engle, I. M., 1997. Mercury's magnetosphere: Another look. Planet. Space Sci. 45 (1), 127–132.

Giampieri, G., Balogh, A., 2001. Modeling of magnetic field measurements at Mercury. Planet. Space Sci. 49, 1637–1642.

Giampieri, G., Balogh, A., 2002. Mercury's thermoelectric dynamo revisited. Planet. Space Sci. 50 (7–8), 757–762.

Glassmeier, K.-H., 2000. Currents in Mercury's Magnetosphere, In Magnetospheric Current Systems (S. Ohtani, R. Fujii, M. Hesse, and R. L. Lysak, Eds.), Geophysical Monograph 118, pp. 371–380. American Geophysical Union, Washington.

Glassmeier, K.-H., N. P. Mager and D. Y. Klimushkin, Concerning ULF pulsations in Mercury's magnetosphere, *Geophys. Res. Lett.*, *30*, SSC 4-1, doi:10.1029/2003GL017175, 2003.

Gold, R. E., Solomon, S. C., McNutt, R. L., Santo, A. G., Abshire, J. B., Acuna, M. H., Afzal, R. S., Anderson, B. J., Andrews, G. B., Bedini, P. D., Cain, J., Cheng, A. F., Evans, L. G., Feldman, W. C., Follas, R. B., Gloeckler, G., Goldsten, J. O., Hawkins, S. E., Izenberg, N. R., Jaskulek, S. E., Ketchum, E. A., Lankton, M. R., Lohr, D. A., Mauk, B. H., McClintock, W. E., Murchie, S. L., Schlemm, C. E., Smith, D. E., Starr, R. D., Zurbuchen, T. H., 2001. The MESSENGER mission to Mercury: Scientific payload. Planet. Space Sci. 49 (14–15), 1467–1479.

Jackson, D. J., Beard, D. B., 1977. The magnetic field of Mercury. J. Geophys. Res. 82 (19), 2828–2836.

Korth, H., B. J. Anderson, M. H. Acuna, J. A. Slavin, N. A. Tsyganenko, S. C. Solomon, R. L. McNutt, Determination of the properties of Mercury's magnetic Field by the MESSENGER mission, *Planet. Space Sci.*, *54*, 733-746, 2004.

Lohr, D. A., L. J. Zanetti, B. J. Anderson, T. A. Potemra, J. R. Haye s, R. E. Gold, R. M. Henshaw, F. F. Mobley, D. B. Holland, M. H. Acuna, J. L. Scheifele, Near Magnetic Field Investigation, Instrumentation, Spacecraft Magnetics and Data Access, Space Science Reviews, 82 (1,2) , 255-281, 1997.

Luhmann, J. G., Russell, C. T., Tsyganenko, N. A., 1998. Disturbances in Mercury's magnetosphere: Are the Mariner 10 "substorms" simply driven? J. Geophys. Res. 103 (A5), 9113–9119.

Ness, N. F., Behannon, K.W., Lepping, R. P., Whang, Y. C., Schatten, K. H., Magnetic field observations near Mercury: Preliminary results from Mariner 10. Science 185 (4146), 151–160, 1974.

Ness, N. F., Behannon, K.W., Lepping, R. P., 1975. The magnetic field of Mercury, 1. J. Geophys. Res. 80 (19), 2708–2716.

Ness, N. F., K. W. Behannon, R. P. Lepping, Y. C. Whang, Observations of Mercury's magnetic field, *Icarus 28 (4)*, 479–488, 1976.
Ogilvie, K. W., Scudder, J. D., Hartle, R. E., Siscoe, G. L., Bridge, H. S., Lazarus, A. J., Asbridge, J. R., Bame, S. J., Yeates, C. M., 1975. Observations at Mercury encounter by the plasma science experiment on Mariner 10. Science 185 (4146), 145–151.
Potter, A. E. and T. H. Morgan, Evidence for Magnetospheric Effects on the Sodium Atmosphere of Mercury, *Science*, New Series, *248*, No. 4957, pp. 835-838, 1990.
Runcorn, S. K., 1975a. An ancient lunar magnetic dipole field. Nature 253 (5494), 701–703.
Runcorn, S. K., 1975b. On the interpretation of lunar magnetism. Phys. Earth Planet. Inter. 10 (4), 327–335.
Russell, C. T., Baker, D. N., Slavin, J. A., 1988. The magnetosphere of Mercury, In Mercury (F. Vilas, C. R. Chapman, and M. S Matthews, Eds.) pp. 494–513. University of Arizona Press, Tucson.
Santo, A. G., Gold, R. E., McNutt, R. L., Solomon, S. C., Ercol, C. J., Farquhar, R. W., Hartka, T. J., Jenkins, J. E., McAdams, J. V., Mosher, L. E., Persons, D. F., Artis, D. A., Bokulic, R. S., Conde, R. F., Dakermanji, G., Goss, M. E., Haley, D. R., Heeres, K. J., Maurer, R. H., Moore, R. C., Rodberg, E. H., Stern, T. G.,Wiley, S. R.,Williams, B. G., Yen, C. L., Peterson, M. R., 2001. The MESSENGER mission to Mercury: Spacecraft and mission design. Planet. Space Sci. 49 (14–15), 1481–1500.
Siscoe, G. L., Christopher, L., 1975. Variations in the solar wind stand-off distance at Mercury. Geophys. Res. Lett. 2 (4), 158–160.
Slavin, J. A., Holzer, R. E., 1979. The effect of erosion on the solar wind stand-off distance at mercury. J. Geophys. Res. 84 (A5), 2076–2082.
Slavin, J. A., J. C. J. Owen, J. E. P. Connerney, and S. P. Christon, Mariner 10 observations of field-aligned currents at Mercury, *Planet. Space Sci. 45 (1)*, 133–141, 1997.
Smith, C.W., Acuna,M. H., Burlaga, L. F., L'Heureux, J., 1998. The ACE magnetic field experiment. Space Sci. Rev. 86 (1–4), 613–632.
Solomon, S. C., 1976. Some aspects of core formation in Mercury. Icarus 28 (4), 509–521.
Solomon, S. C., McNutt, R. L., Gold, R. E., Acu˜na, M. H., Baker, D. N., Boynton, W.V., Chapman,C. R.,Cheng,A. F., Gloeckler,G., Head, J.W.,Krimigis,S. M., McClintock, W. E., Murchie, S. L., Peale, S. J., Phillips, R. J., Robinson, M. S., Slavin, J. A., Smith, D. E., Strom, R. G., Trombka, J. I., Zuber, M. T., 2001. The MESSENGER mission to Mercury: Scientific objectives and implementation. Planet. Space Sci. 49 (14–15), 1445–1465.
Srnka, L. J., 1976. Magnetic dipolemoment of a spherical shell with TRM acquired in a field of internal origin. Phys. Earth Planet. Inter. 11 (3), 184–190.
Stephenson, A., 1976. Crustal remanence and the magnetic moment of Mercury. Earth Planet. Sci. Lett. 28 (3), 454–458.
Stevenson, D. J., 1983. Planetary magnetic fields. Rep. Prog. Phys. 46 (5), 555–620.
Stevenson, D. J., 1987. Mercury's magnetic field: A thermoelectric dynamo? Earth Planet. Sci. Lett. 82 (1–2), 114–120.
Stevenson, D. J., Spohn, T., Schubert, G., 1983. Magnetism and thermal evolution of the terrestrial planets. Icarus 54 (3), 466–489.
Whang, Y. C., 1977. Magnetospheric magnetic field of Mercury. J. Geophys. Res. 82 (7), 1024–1030.

Tables

Table 1. MESSENGER magnetometer resources and performance characteristics.

Dimensions:	Sensor	8.1cm x 4.8cm x 4.6cm	
	Electronics	13.0cm x 10.4cm x 8.6cm	
	Boom	3.6 m long	
Mass:	Sensor:	184g	
	Electronics:	835g	
	Boom	2.66kg	
	Cable:	408g	
	Total:	4.09kg	
Power:	Instrument	4.2 W	
	Probe heater	0.93 W (2 W limited)	
Type:	Low noise tri-axial fluxgate (< 20 pT intrinsic noise level)		
A/D:	20-bit, 20 conversions/second		
	Self calibrating on command		
	Three independent units, one dedicated for each axis		
Ranges:	Coarse	±51,300 nT full scale	1.56 nT resolution (16 bits out)
	Fine	±1,530 nT full scale	0.047 nT resolution (16 bits out)
Output Rates:	Maximum:	20/s (10 Hz analog filter) - internal A/D	
	Filtered:	10/s, 5/s, 2/s, 1/s (digital filter at Nyquist frequency)	
	Sub-sampled:	0.5/s, 0.2/s, 0.1/s, 0.05/s, 0.02/s, 0.01/s (0.5 Hz filter)	
Output Data Volume:	Vector field:	48 bits per three axis sample	
	AC channel:	8 bits log compressed per sample (one axis)	
	Packet avg.:	56.5 bits per sample (before compression)	
	Compression:	lossless differential pulse code modulation (DPCM)	

Table 2. Absolute gain, sensor alignment calibration values, and internal instrument offsets.

Parameter	Coarse range (±51,300 nT)	Fine range (±1,530 nT)
k_x: nT/count	**1.56513**	**0.046769**
k_y: "	**1.56419**	**0.046673**
k_z: "	**1.61029**	**0.047997**
α	**-0.00462**	**-0.00462**
β	**0.00053**	**0.00053**
γ	**-0.00736**	**-0.00736**
X offset: counts (nT)	**-30.4 (-48)**	**-1017 (-48)**
Y offset: "	**-75.2 (-102)**	**-2520 (-102)**
Z offset: "	**-16.2 (-26)**	**-544 (-26)**

Table 3. MESSENGER Magnetometer sample rates, digital IIR filter –3dB points, filter attenuation characteristics, IIR time lags and net time lags.

Rate setting	Sample rate (1/sec)	Filter: -3dB (Hz)	Attenuation (dB/octave)	IIR Lag (sec)	Net Lag (sec)
0	0.01	0.567*	-72*	2.316	2.358
1	0.02	"	"	"	"
2	0.05	"	"	"	"
3	0.10	"	"	"	"
4	0.20	"	"	"	"
5	0.50	"	"	"	"
6	1.00	"	"	"	"
7	2.0	1.141*	-73*	1.144	1.186
8	5.0	2.83*	-97*	0.435	0.477
9	10.0	5.38*	-147*	0.181	0.223
10	20.0	11.3	-17	0.0	0.042

* Characteristics of IIR digital filter.

Figures

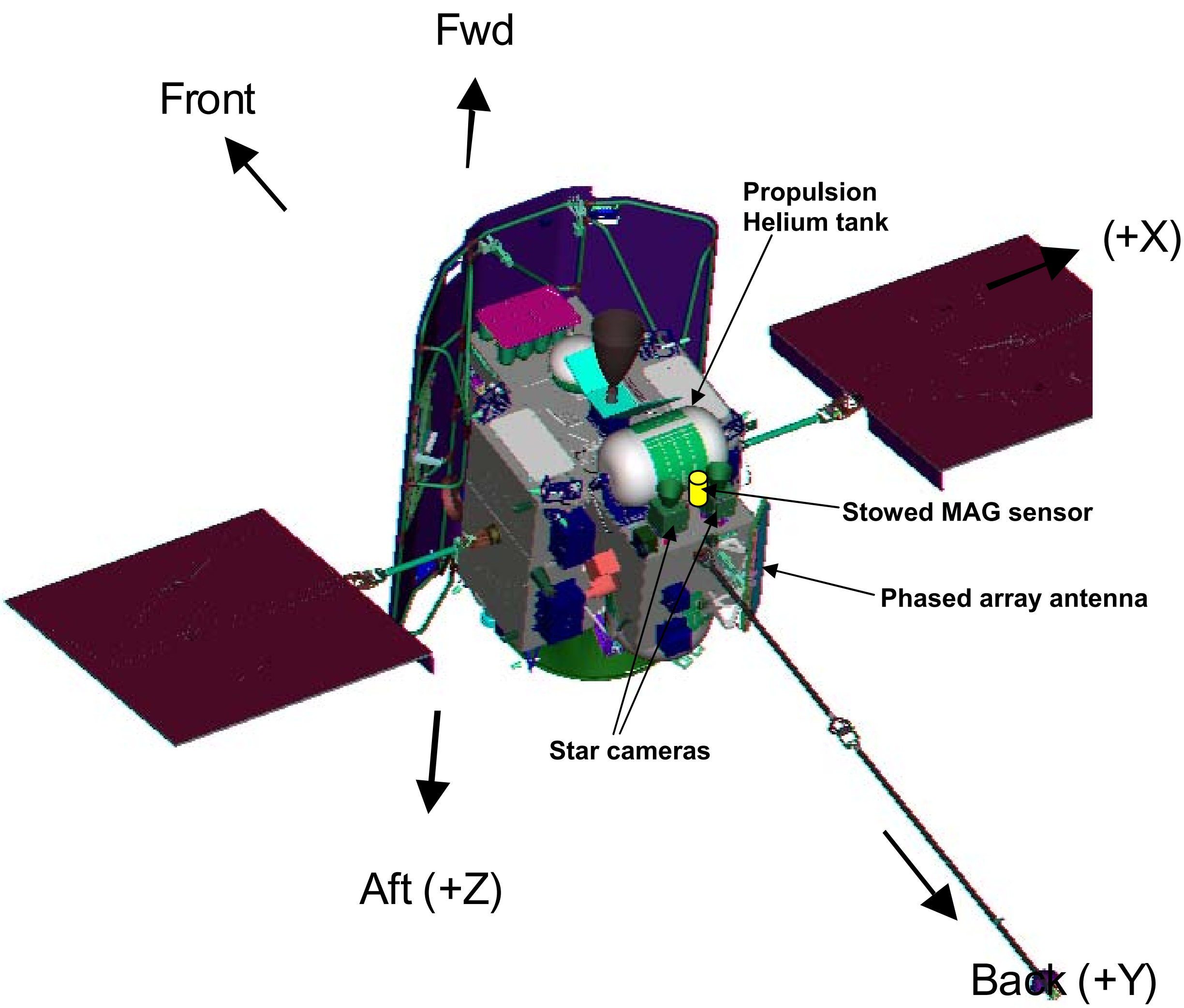

Figure 1. MESSENGER spacecraft showing the instrument coordinates and the magnetometer boom deployed in the +Y direction which is the anti-sunward direction during orbital operations. The MAG sensor stowed location is indicated (yellow cylinder) as are the propulsion system Helium tank, star cameras and the phased array antenna nearest the stowed magnetometer sensor. The spacecraft sunshade is on the –Y side of the vehicle, facing 'front' as labeled in the figure.

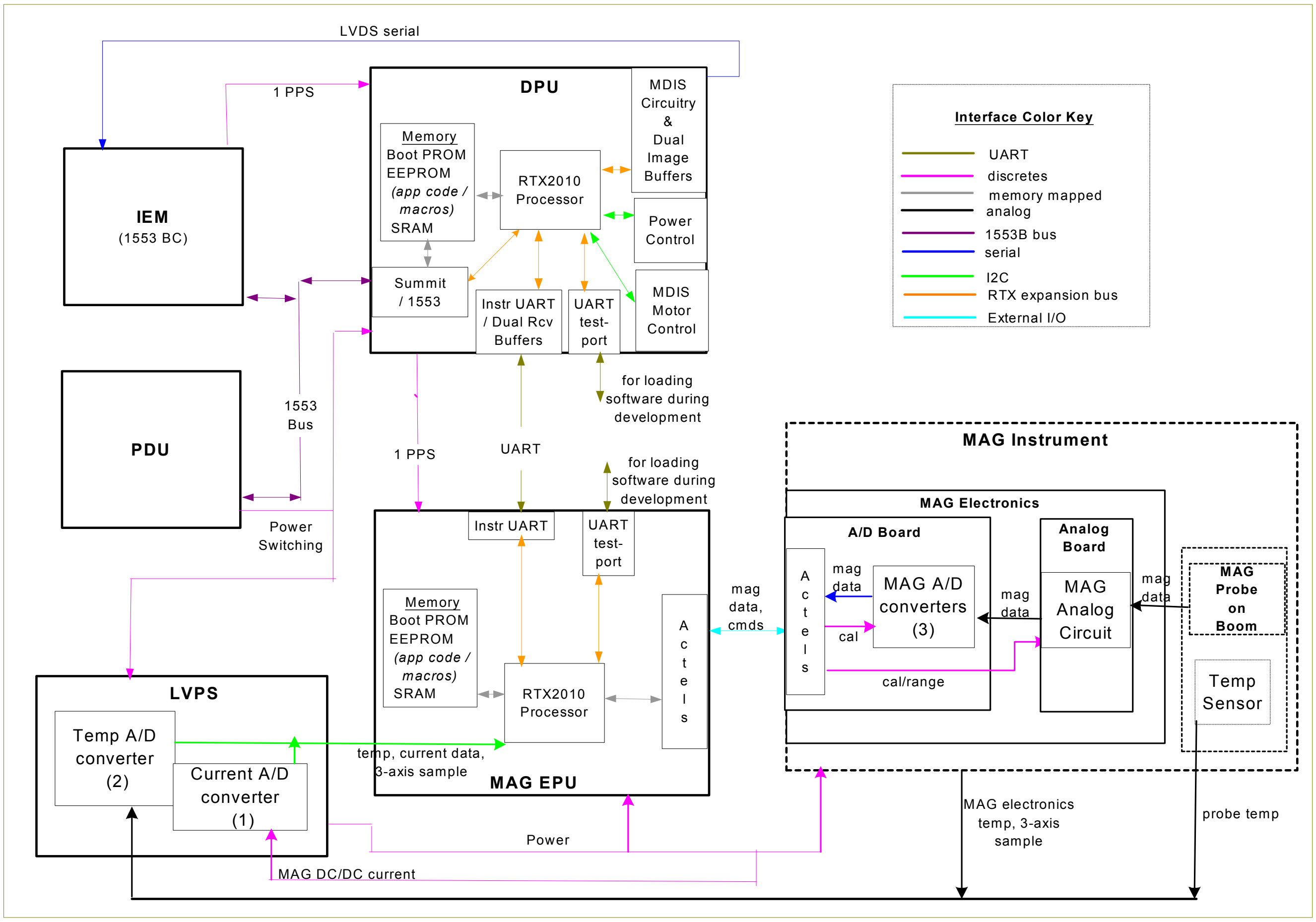

Figure 2. MESSENGER Magnetometer Instrument Block Diagram showing the DPU, EPU, MAG digital and analog electronics, LVPS and their interfaces.

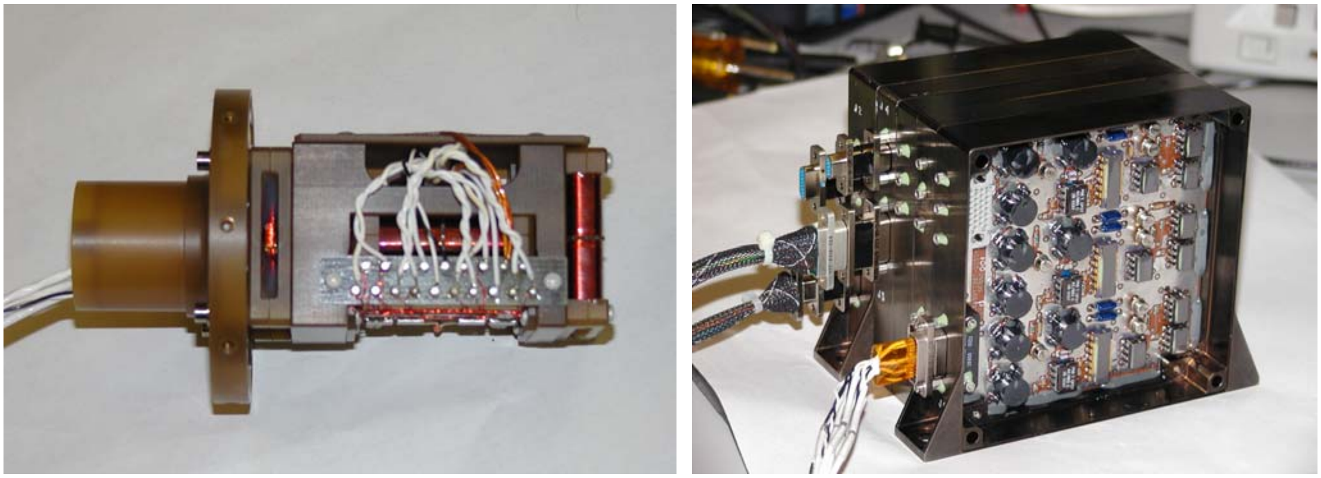

Figure 3. Flight MESSENGER MAG sensor (left) and electronics (right) with view of analog slice. The sensor is shown mounted to a test boom adapter flange. Sensor dimensions not including the flange are 8.1 cm x 4.8 cm x 4.6 cm. The electronics dimensions are 10.4 cm and 8.6 cm in cross section as shown and 13.0 cm deep.

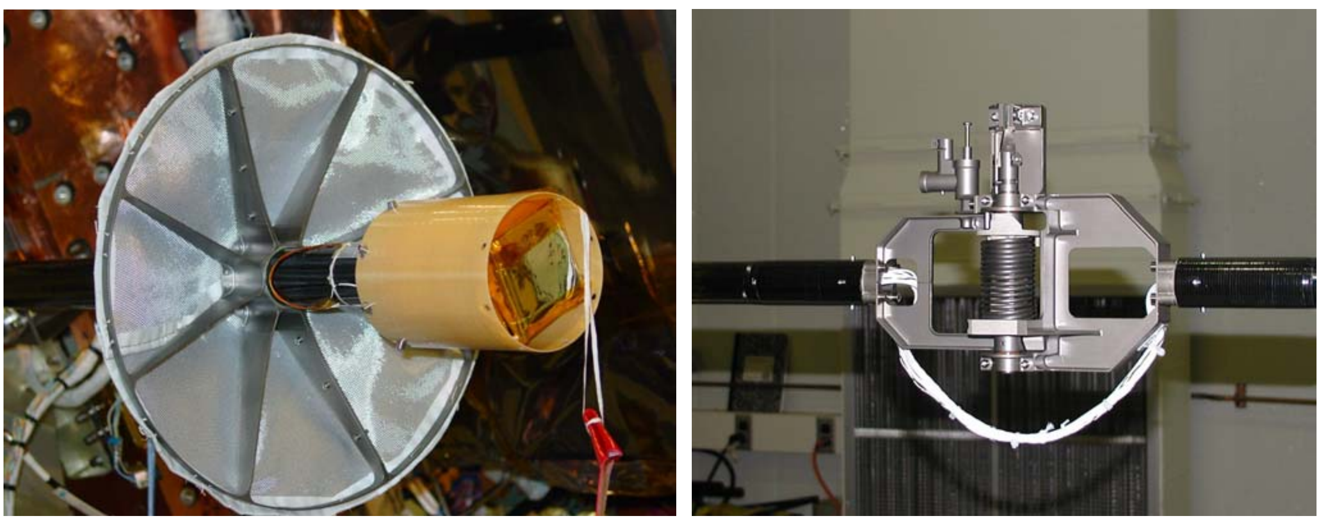

Figure 4. Flight MESSENGER MAG sensor and sensor sun shade integrated to the boom and spacecraft prior to final thermal blanketing (left) and MAG boom midpoint hinge (right) during deployment testing prior to installation of thermal blankets.

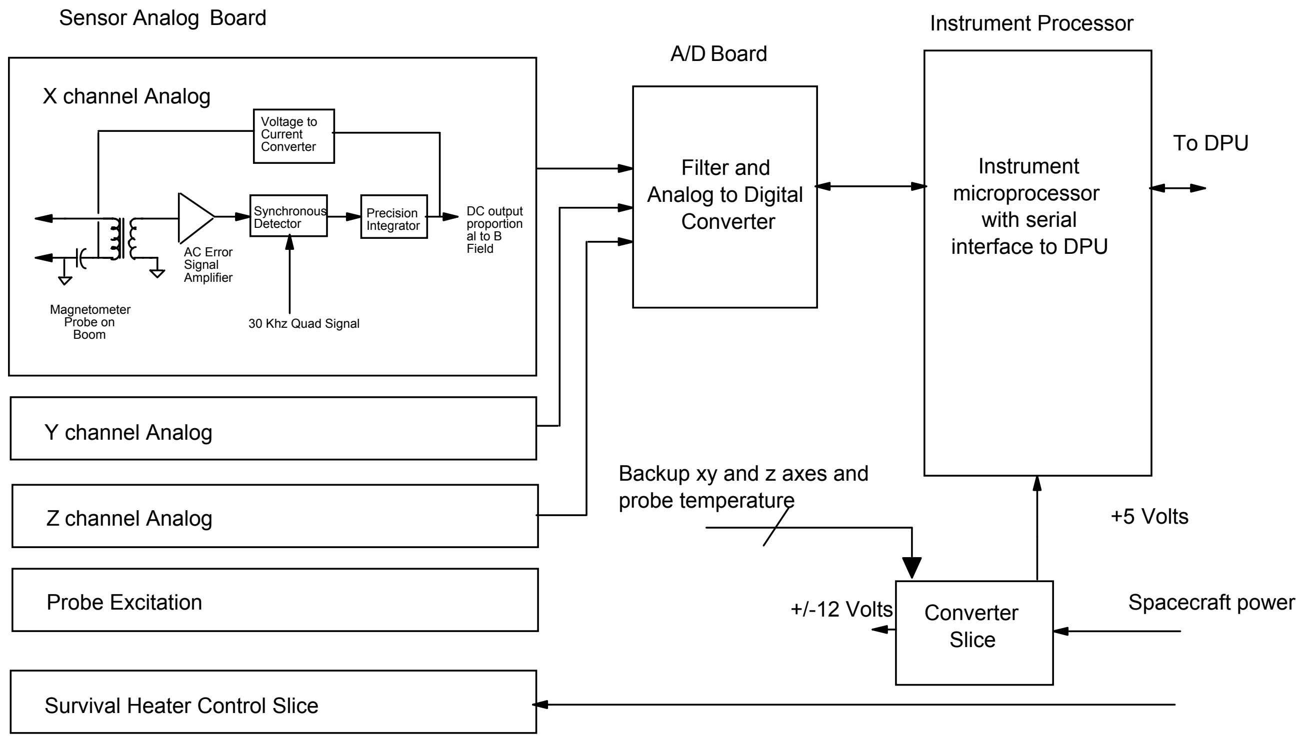

Figure 5. Magnetometer electronics functional schematic showing the three independent synchronous detection sense circuits, one for each axis and the functional interfaces between the A/D converter, MAG EPU, power supply and thermostatic sensor heater control.

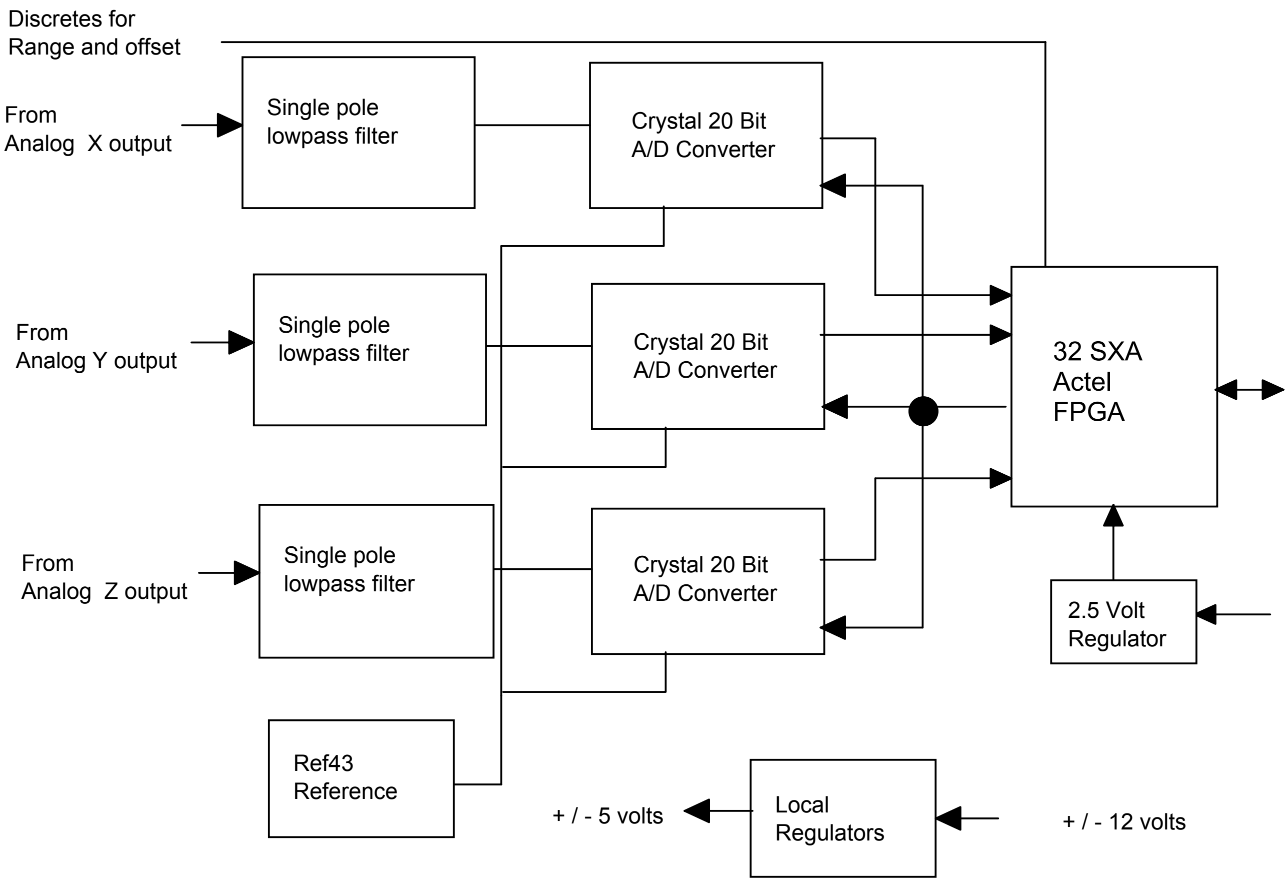

Figure 6. MAG A/D conversion electronics functional schematic showing the three independent anti-alias analog filters, three 20-bit A/D converters and the conversion trigger/data buffer FPGA interfaces.

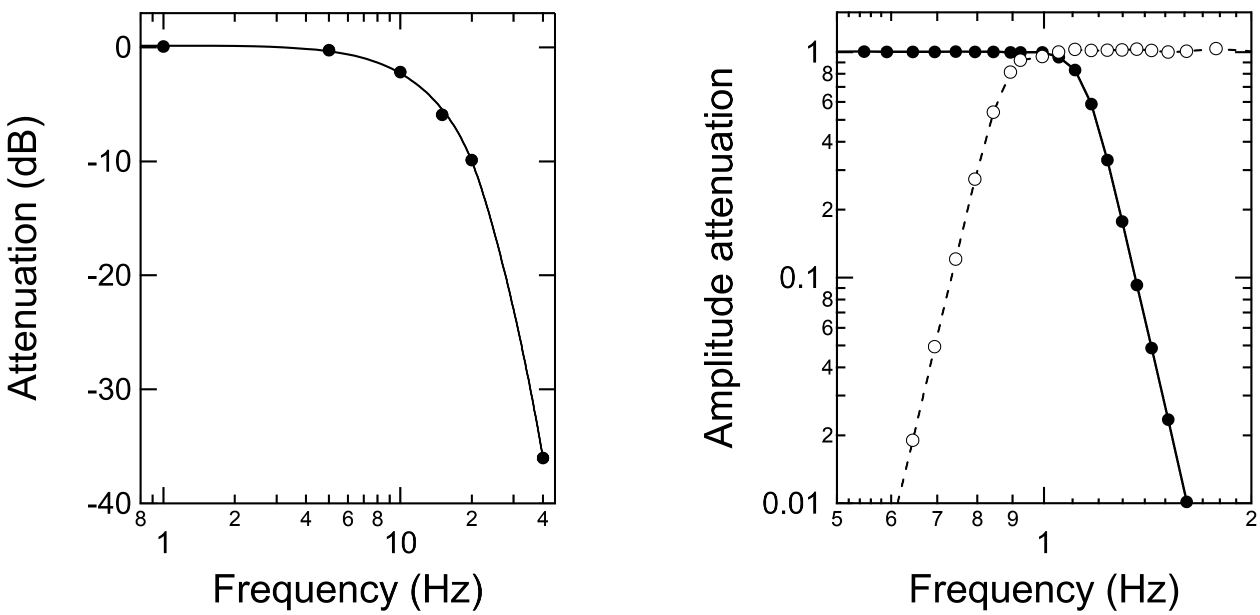

Figure 7. Frequency response of attenuation of analog electronics and A/D low pass anti-aliasing filter (left), and digital filters (right). The analog anti-alias filter has its –3 dB point at 11.3 Hz, –17 dB/octave at 15 Hz. The 1 Hz low pass (solid symbols) and 1 Hz high pass (open symbols) IIR digital filters (right) characteristics are –3 dB at 1.14 Hz, –73 dB/octave above 1.25 Hz and –3 dB at 0.87 Hz, –75 dB/octave below 0.8 Hz, respectively.

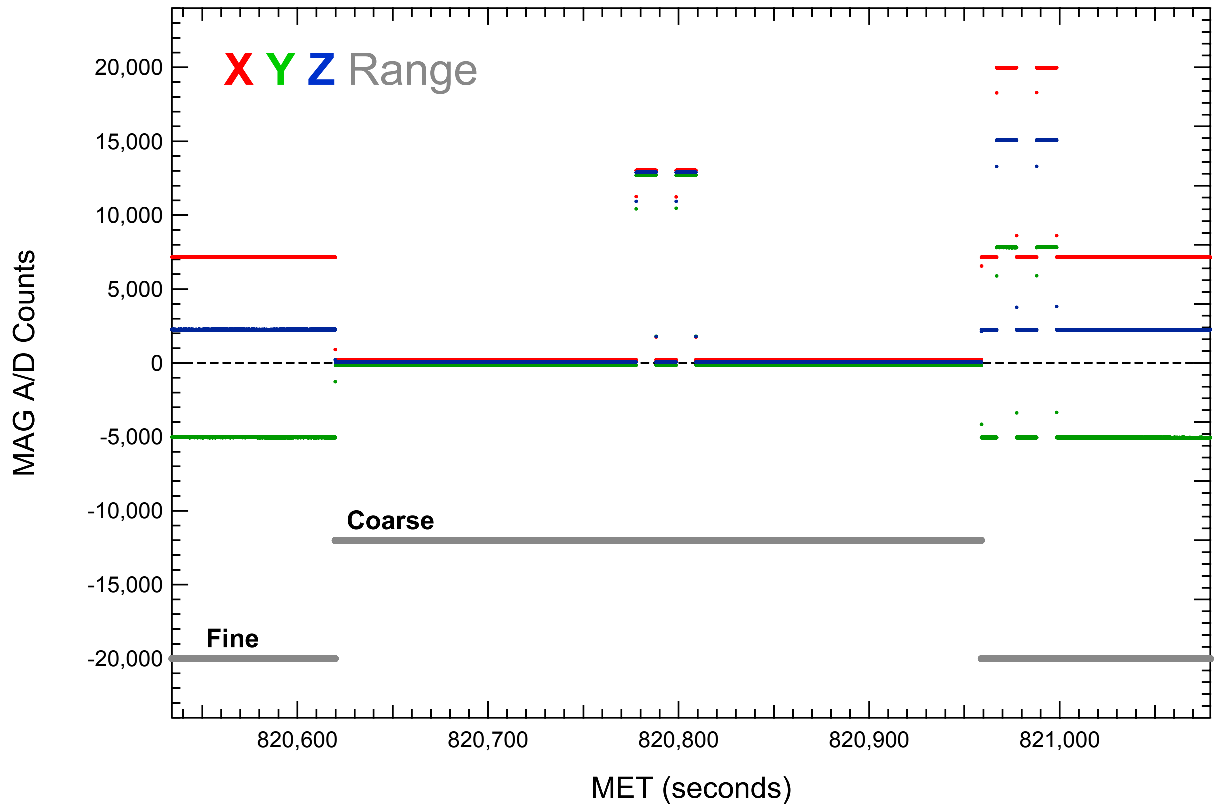

Figure 8. First in-flight data from the MESSENGER MAG on 12 August 2004, nine days after launch. Plot shows initial checkout operations including analog calibration and range commanding. The two square wave pulses near 820,800 MET and 821,000 MET are activations of the analog calibration. One major division is 235 nT. The magnetometer remained stowed until 8 March 2005.

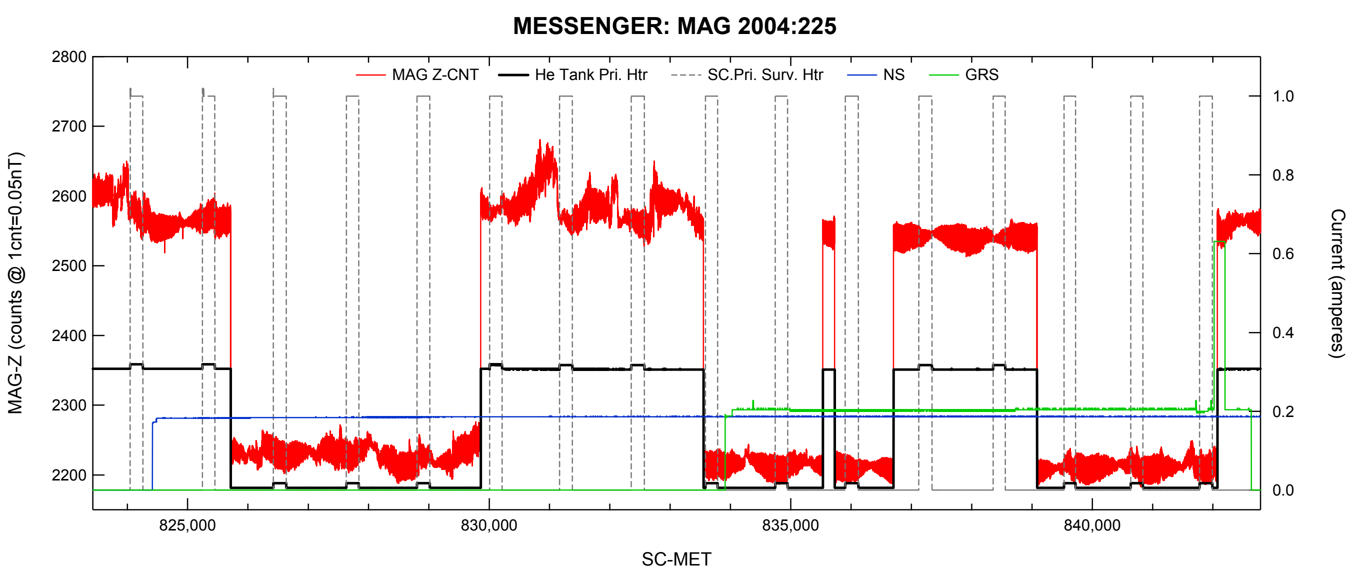

Figure 9. MESSENGER MAG Z-axis data in counts (red trace, left axis) and spacecraft housekeeping currents (right axis) for the NS and GRS initial turn on sequences on 12 August 2004. The ~20 nT square waves in Z are clearly due to the propulsion Helium tank heater current (the primary spacecraft survival heater is aliased into the Helium heater reading). No magnetic signals were observed for NS or GRS activities.

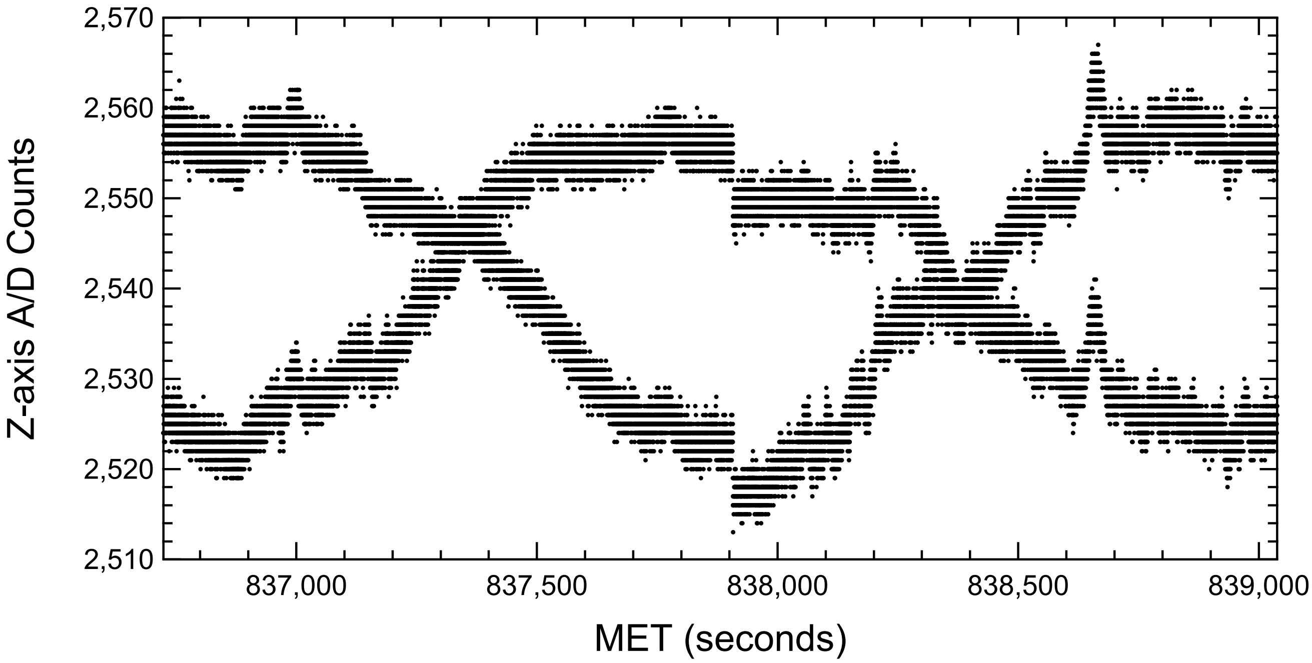

Figure 10. Expanded view of beat signal in Z-axis from day 225. Each sample is plotted by a dot which reveals a clear 'double banded' signature in the signal.

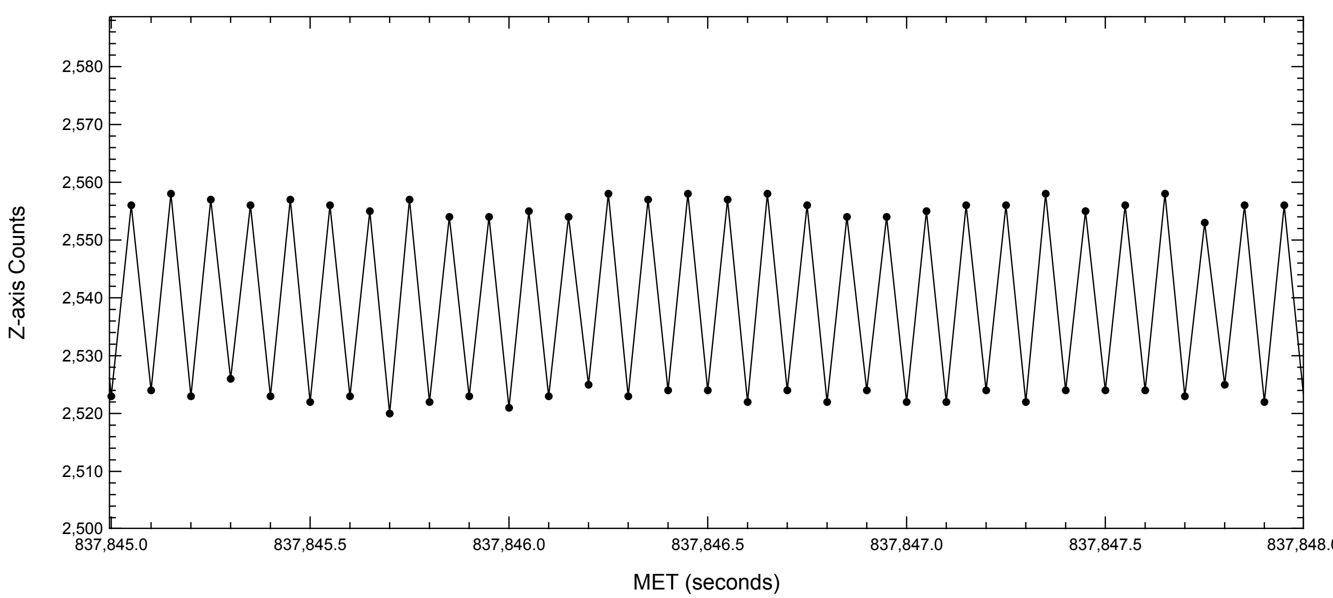

Figure 11. Detailed view showing three seconds of data from the Z-axis on day 225 near the maximum of a beat amplitude. Lines are plotted between points showing clearly that the doubled banded signature is due to oscillation between extremes of the beat amplitude indicative of a signal near 10 Hz.

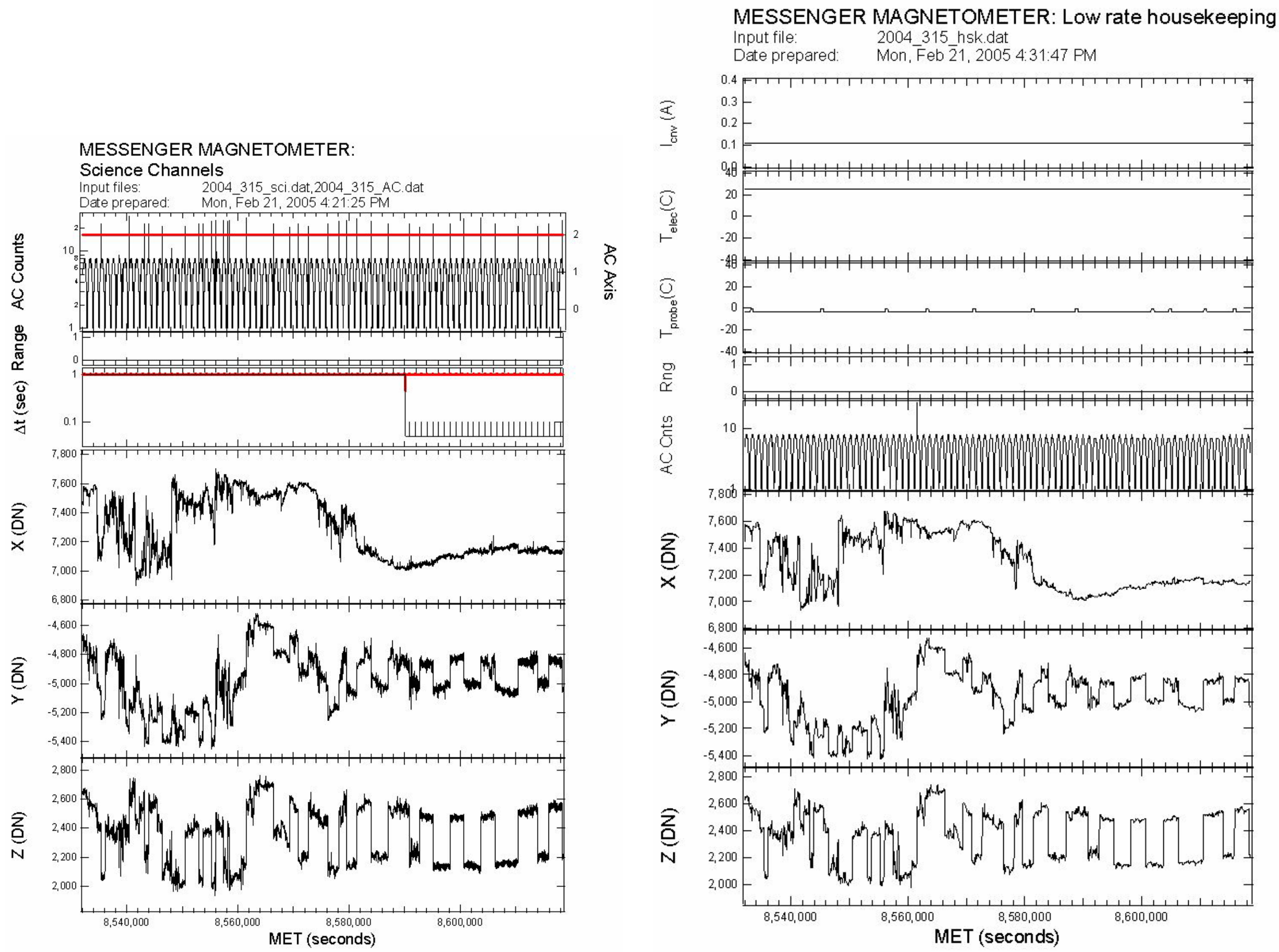

Figure 12. Quick look summary plots for 10 November 2004, day 315, for the standard science data (SSD) on the left, and the low rate housekeeping (LHK) data on the right. From top to bottom the SSD plot shows: the logAC counts and the AC axis (red trace, right hand scale, X=0, Y=1, Z=2); the instrument range (fine = 0, coarse = 1); the time increment between consecutive vector samples (black trace) and logAC samples (red trace); the X, Y and Z axis magnetic field values in counts. From top to bottom the LHK plot shows: the instrument current; the electronics temperature; the probe temperature; the instrument range; the logAC values; and the X, Y and Z axis magnetic field values in counts.

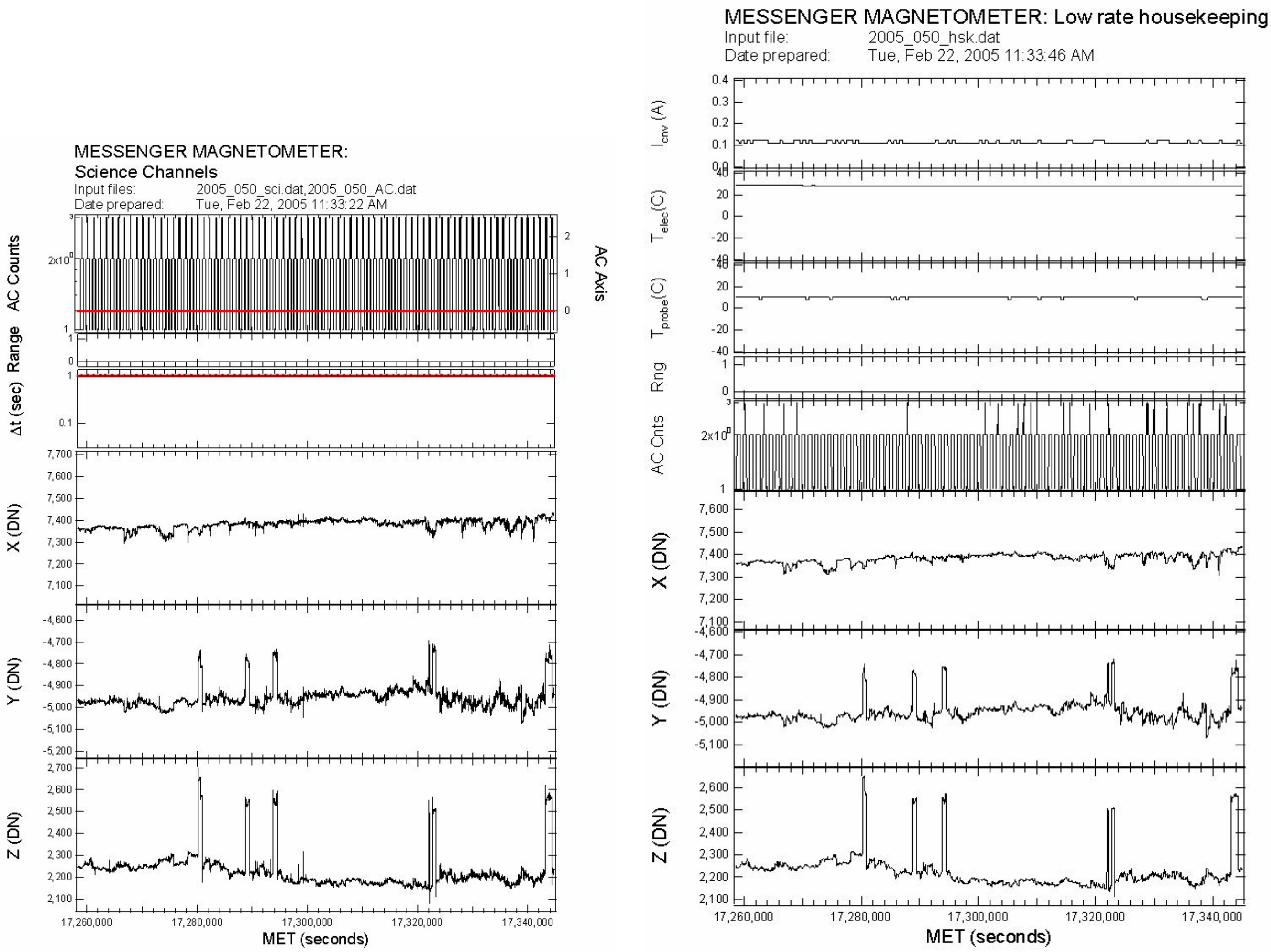

Figure 13. Quick look summary plots for 19 February 2004, day 50, in the same format as Figure 12.